# SOURCE MECHANISM INVERSION OF VERY LONG PERIOD SIGNALS ASSOCIATED WITH STROMBOLIAN ERUPTIONS AT MOUNT EREBUS, ANTARCTICA

by

Sara McNamara

Submitted in Partial Fulfillment
of the Requirements for the Degree of
Master of Science in Geophysics

New Mexico Institute of Mining and Technology
Socorro, New Mexico
August, 2004

# ABSTRACT

Since 1996, oscillatory, very long period (VLP) ($25 > T > 5$ s) seismic signals have been recorded at Mount Erebus by near-field broadband seismometers and found to be ubiquitously and uniquely associated with Strombolian eruptions. The VLP signal begins before there is any visible surface indication of an eruption and continues throughout the eruption and conduit recovery process. The eruptions occur as large gas bubbles (up to 10-m diameter) explosively decompress at the surface of a lava lake, eviscerating the lake in the process. After the eruption the lava lake recharges and resumes its pre-eruption appearance. VLP and short-period waveforms are all highly similar from event to event, suggesting that the source mechanism is repeatable and non-destructive, or self-recreating. However, the initial vertical displacement polarity of the events may be either positive or negative, as is visible in systematic differences associated with two different eruptive styles seen in the first 5-10 seconds of seismograms. To better understand the VLP source forces and associated volcanic processes during the eruptions and lava lake recharge period, moment tensor inversion on high signal-to-noise stacked data as well as for single events has been performed. Seismograms from up to eight broadband stations with three components were used in the inversion. Increasing degrees of model freedom, ranging from a pure Mogi (implosive/explosive) source up to six individual source time functions (one for each moment tensor element) and a single vertical force were considered. The volumetric moment tensor element ratio of approximately [1:1:3] is generally consistent with a subhorizontal crack mechanism. The source centroid is shallow (around 100 meters). Inversions also revealed that the positive polarity event requires a larger single force than the negative polarity event. The single force for the positive event is also necessary for the entire duration of the seismic signal, even initial pre-eruptive stages. However, for the negative polarity event, the single force is greatly reduced for the initial several seconds. These differences are partly explained by video analysis of these two types of eruptions. The results suggest at least two distinct source regions existed for Erebus Strombolian eruptions during 1996-2002.

# ACKNOWLEDGMENT

I would like to thank my advisor, Rick Aster, for his guidance and knowledge. The graduate students in the Geophysics program never failed to give me help and support. Sue Bilek was a great help for her comments on this paper. Matt Richmond was a tremendous source of both technical and moral support. And I'd like to thank my family for bringing me this far.

NSF Office of Polar Programs grants OPP-9814291, OPP-0116577, OPP-022935 supported this research. Instrumentation was provided by the IRIS PASSCAL Instrument Center.

This report was typeset with LaTeX[1] by the author.

---

[1] LaTeX document preparation system was developed by Leslie Lamport as a special version of Donald Knuth's TeX program for computer typesetting. TeX is a trademark of the American Mathematical Society. The LaTeX macro package for the New Mexico Institute of Mining and Technology report format was adapted from Gerald Arnold's modification of the LaTeX macro package for The University of Texas at Austin by Khe-Sing The.

# TABLE OF CONTENTS

# LIST OF TABLES

# LIST OF FIGURES

This report is accepted on behalf of the faculty of the Institute by the following committee:

Richard C. Aster, Advisor

Sara McNamara

Date

# CHAPTER 1

## Introduction

Mount Erebus is a stratovolcano located at Ross Island, Antarctica. It has phonolitic lava and strombolian style eruptions. Mt. Erebus has an elevation of 3794 m and a volume of approximately 1670 km$^3$ [Aster et al., 2003]. Above $\sim$3500 m, the volcano has a summit plateau surrounding a summit cone, which in turn contains a Main Crater and an Inner Crater. The plateau is composed of interbedded lava flows and phonolitic pyroclastic bomb deposits. It has been in almost continual eruption since its discovery in 1841 by James Clark Ross.

A phonolitic lava lake resides within the Inner Crater and has a radius which has varied over the past ten years from approximately 5 to 20 m [Aster et al., 2003]. The convecting lava lake has persisted for at least three decades, aside from a few months in 1984 when it was buried by eruptive debris [Aster et al., 2003]. Lava lakes persisting over long periods are very unusual and only a handful have ever been reported (examples include Nyiragongo, Zaire and Erta 'Ale, Ethiopia [Rothery and Oppenheimer, 1994]). The fact that the lava lake has not solidified shows that the volcano is in a constant state of convective conduit activity [Tazieff, 1994].

Mt. Erebus Volcano Observatory (MEVO) was established in 1992 to monitor and study the volcano [Rowe et al., 2000]. Short-period seismic stations have helped in the monitoring of Mt. Erebus since 1980. In 1996, three temporary IRIS PASSCAL broadband sensors were deployed [Rowe et al., 2000]. In the 1999-2000 field season, there was a two month deployment of eight IRIS PASSCAL broadband stations in the near field (0.7-2.5 km) of the summit [Aster et al., 2003]. In subsequent years, permanent broadband stations were installed with six currently operating stations. Seismic monitoring is complimented by GPS and tilt measurements, three stations have infrasound, one station has infrared, and a continuously recording video camera is aimed at the lava lake (Figure 1.1) [Aster et al., 2004].

The strombolian eruptions on Mt. Erebus are initiated by a gas slug. This slug is first trapped within the conduit, presumably by a physical barrier, at a depth of no more than a few tens of meters. Once the slug breaks loose of its barrier, it rises to the surface of the lava lake, where it decompresses explosively and sprays lava and lava bombs around the crater. These slugs have been observed by video observation to be up to 5 m in radius [Aster et al., 2003]. After the explosive eruption, the lava lake is eviscerated and begins recharging.

Broadband stations revealed Very Long Period (VLP) (25 s >T> 5 s) signals invariably associated with explosion events (Figure 1.2) [Aster et al., 2003]. As seen in video observations, the signals begin seconds before there is any surface indication of an eruption and continue for several minutes until the lava lake reaches equilibrium and the coda becomes indistinguishable from noise levels. The relative onset time of the signals varies, but on high signal-to-noise signals, it has been seen up to 5 seconds before the explosion. The seismic signal is not in phase with the surface features of the lava lake, showing

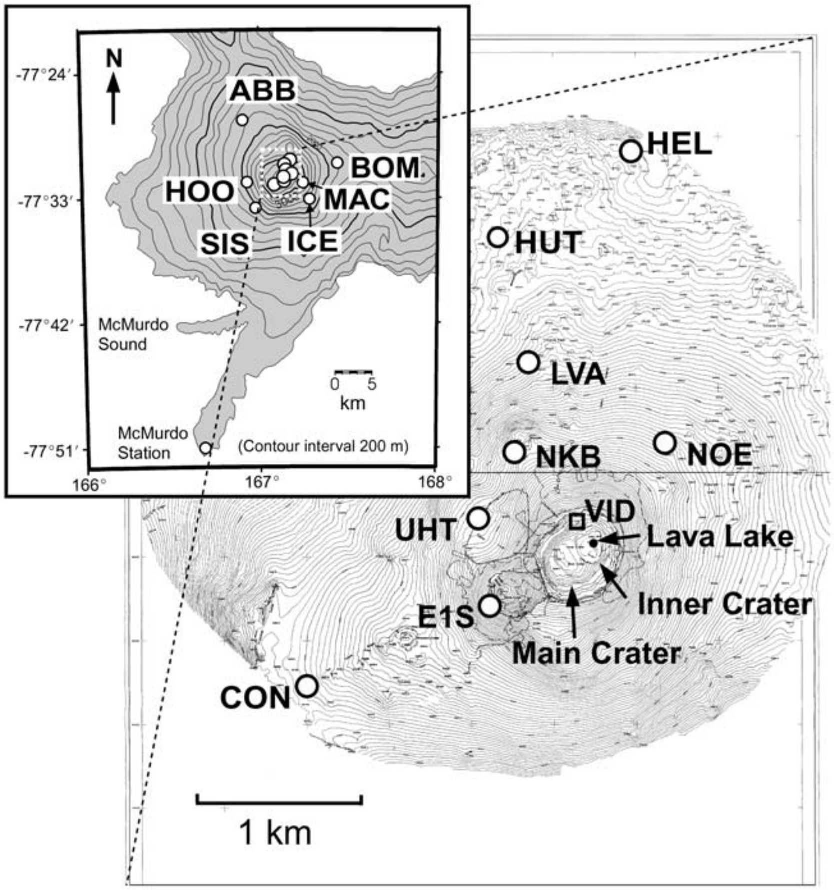

Figure 1.1: Mount Erebus, showing topography and seismic stations. Inset shows short period stations and expanded view shows broadband stations and the location of the video camera (VID) (after Aster et al., 2003).

that the seismicity is not a consequence of surface activities [Mah, 2003]. VLP signals were found only in association with the strombolian explosions from the inner crater. Prolonged ash eruptions from other vents do not have an associated VLP signal [Mah, 2003].

Broadband observation on volcanoes is still relatively new as broadband seismometers have only recently become easily portable and economical [Aster et al., 2003]. This new monitoring is revealing VLP signals at many volcanoes. Conversely, some volcanoes show a lack of any such signal.

VLP signals found at some volcanoes (e.g. Stromboli [Chouet et al., 2003] and Popocatepetl [Arciniega-Ceballos et al., 1999]) have been found to be associated with eruptions, as with Erebus. However, some volcanoes have VLP signals associated with inflation or dome growth (e.g. Miyake [Kumagai et al., 2001] and Merapi [Hidayat et al., 2002]). Other persistently active volcanoes do not seem to produce VLP signals at all (e.g. Karymsky [Johnson et al., 2003] and Arenal [Hagerty et al., 2000]). Ideally, the study of VLP signals at a volcano should lead to new insights on the plumbing and eruptive processes of that particular volcano.

However, similarities exist among all volcanoes which produce VLP signals. Investigations of the source mechanisms of VLPs point toward a fluid transport origin. Gas or magma movement through a crack is involved in the likely fundamental explanation for each of the observed signals mentioned above. This will be discussed in further detail later.

VLP signals observed at Erebus are highly repeatable, not just from station to station but also from event to event, well into their coda. The ampli-

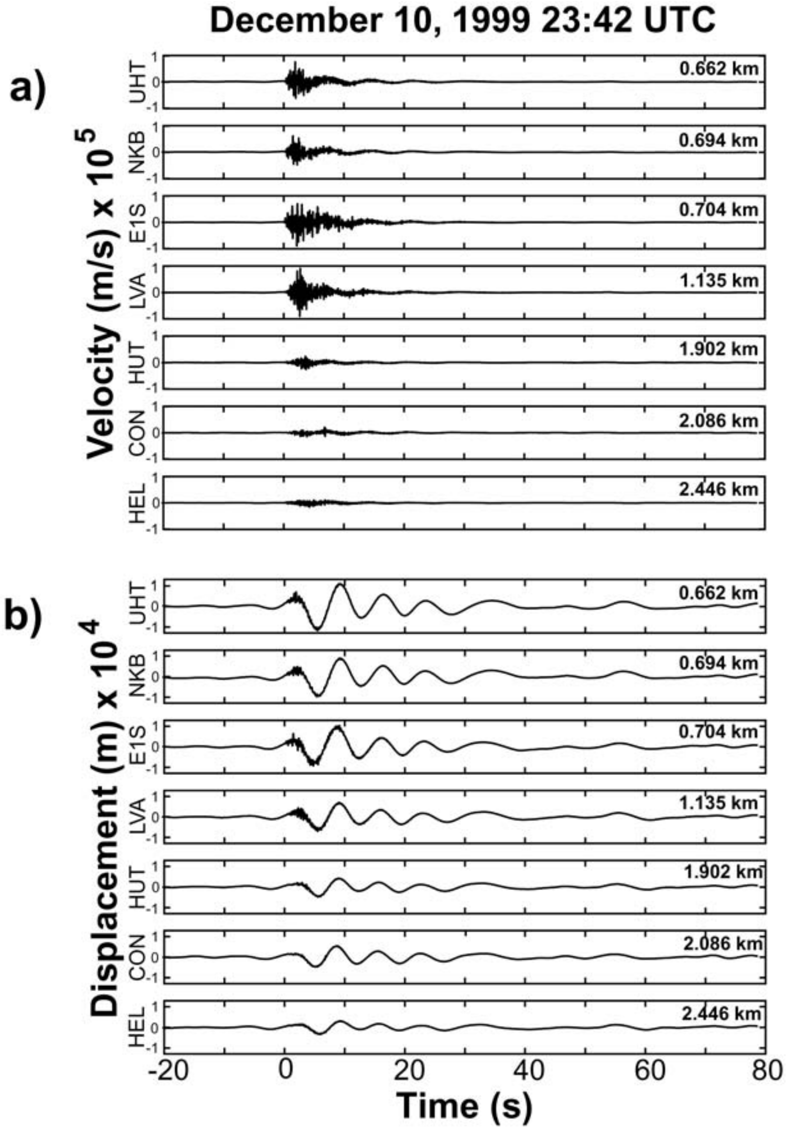

Figure 1.2: Very Long Period signals recorded on the vertical component at Mt. Erebus, associated with a strombolian eruption in December 1999. The time scale is relative to the short period eruption onset time. The sampling rate is 40 samples per second. a) Broadband velocity seismograms with the distance to the station shown at right. b) Signals from a), integrated to displacement and high pass filtered with a corner of 30 s (after Aster et al., 2003).

tude, timing, and initial 5-10 seconds of the signals are variable, but the waveforms are highly similar thereafter (Figure 1.3). The signals consistently show three dominant spectral peaks near 7, 11 and 21 s [Aster et al., 2003]. The similar nature of the signals implies that the source is repeatable and nondestructive or self-generating [Aster et al., 2003]. The small amount of variation between signals from different stations arises because of the very long-wavelengths of the near-field VLP signals [Rowe et al., 2000].

Three different VLP signal types have been identified. Station E1S was primarily used to identify the signal types because it typically has the highest signal-to-noise ratio, is the longest-running broadband station, and is one of the closest to the lava lake (0.7 km) [Mah, 2003]. Two types are similar and are distinguished by their initial onset polarity, being either positive or negative (see Figure 1.4). The initial VLP pulse (positive or negative) also varies in timing by several seconds relative to the eruption. The remaining signal type is more pulse-like in character and very rare with only a few examples observed [Mah, 2003]. Due to the low number of observations, no event suitable for inversion was found and so this event type is not investigated in this study. These similarities between the first two types suggest that, after the first few seconds, the VLP process is nearly the same. This observation suggests one of two scenarios. One possible scenario is that there are two source locations from which the gas bubble is originating, but that the bubbles take the same path up the conduit, and result in the same recharging process. The second possible scenario is that the source location is the same and there are differences in the shape or velocity of the gas bubble, but again the recharging process would not change. This scenario, however, would suggest that a continuum of types would

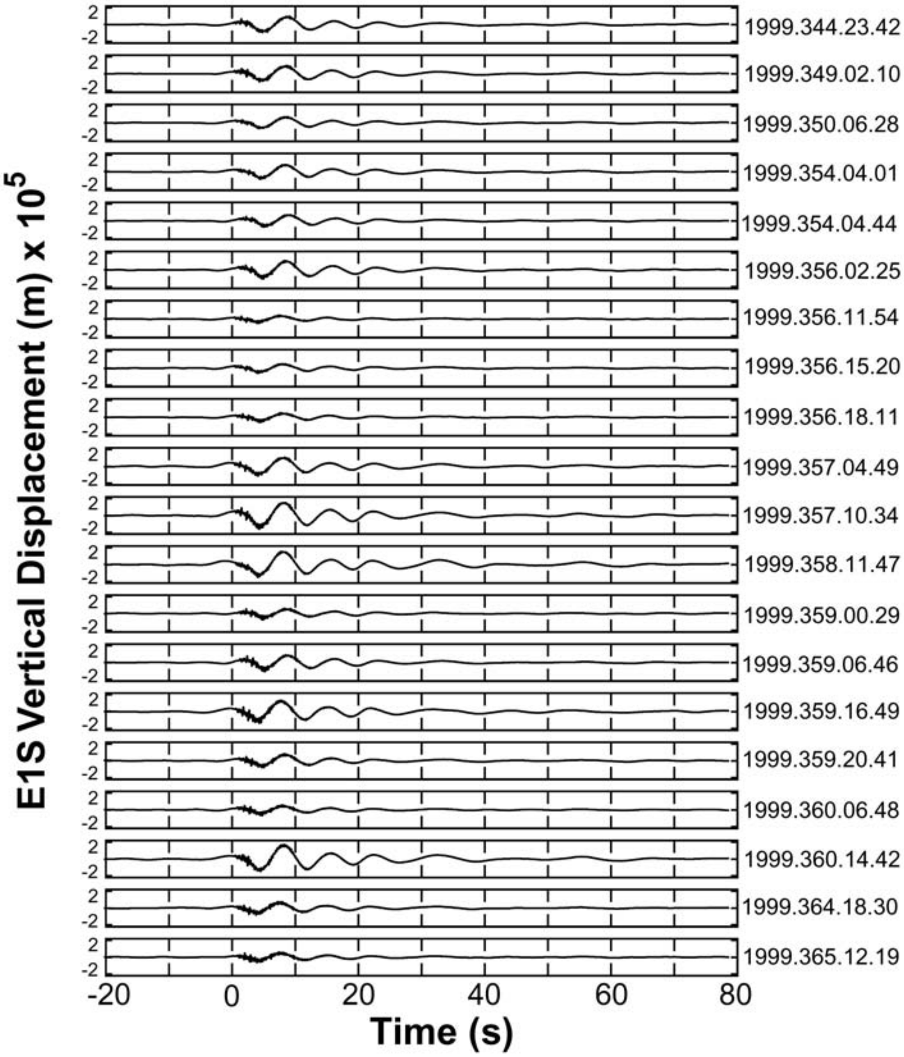

Figure 1.3: Twenty vertical displacement seismograms recorded at station E1S during the 1999-2000 field season. The waveforms are highly similar from event to event, aside from their amplitudes. Displacements can range over a factor of 25 (after Aster et al., 2003).

occur, which is not the case. Previous work by Mah [2003] looking at incident angles of events showed that the incident angles have not varied significantly from the period of 1999 to 2002, indicating that the source location is stable.

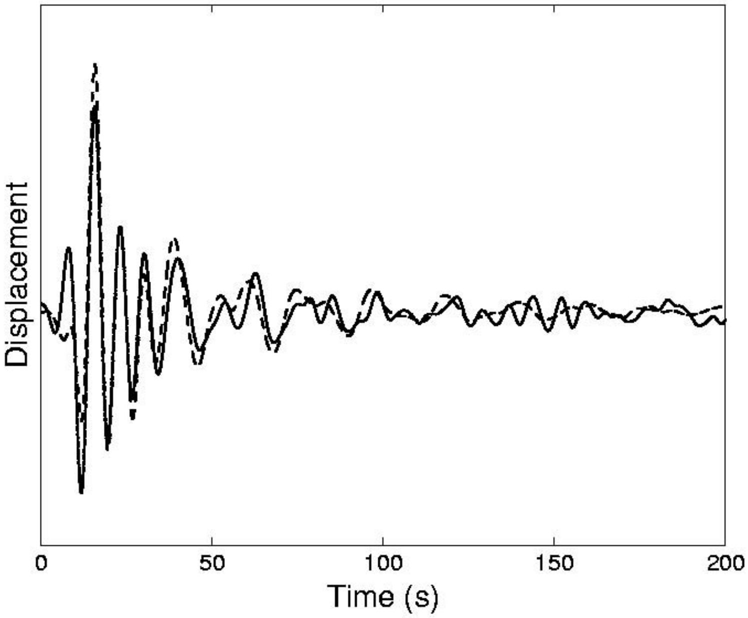

Figure 1.4: Group 1 (first motion positive) event of December 10, 1999 for station E1S shown in solid line. Group 2 (first motion negative) event of January 16, 2000 for station E1S shown in dashed line.

In this study, source mechanism inversion of the VLP signals is performed in order to gain a better understanding of the inner workings and mechanics of Erebus. The inversion provides information about the dominant moment tensor components and their ratios. The moment tensor components characterize a general source as a point-source superposition of forces and force couples. The ratios of the tensor elements give information on the specific mechanism involved, for example, an expanding crack versus an isotropic source.

Work by a former New Mexico Tech student [Mah, 2003] included stacking signals to produce composite seismograms with a high signal-to-noise ratio. These signals will be used for the initial inversion of the VLP coda. The stacks were made for eight broadband stations with three components. These stacks have been normalized and do not therefore provide good representations of either the positive or negative polarity case. Separate inversions will thus also be performed on a sample of individual (and lower signal-to-noise) positive and negative polarity events to assess their moment tensor differences.

# CHAPTER 2

## Data

Broadband seismometers on Erebus have recently been permanently deployed [Aster et al., 2004] and 6 stations are running (when conditions permit). The stacked data used in this study for several moment rate tensor determinations for the VLP coda is from the eight stations that were temporarily deployed during the 1999-2000 field season. Not only was there better station coverage during this two-month deployment, but Erebus was more active during that time than currently. The 1999-2000 deployment used Guralp 3ESP and CMG 3T instruments from the IRIS PASSCAL instrument pool, and was supported by the IRIS PASSCAL Instrument Center at New Mexico Tech.

The 1999-2000 stations provide nearly 180 degree azimuthal coverage across the northern summit plateau. The southern side of the mountain is steep and covered in ice which makes it much more difficult to place stations there.

All seismograms were filtered with a highpass zero-phase four-pole filter with a corner of 30 s, integrated from velocity to displacement, and then lowpass filtered at 5 s [Aster et al., 2003]. The number of events for each stacked seismogram is given in Table 2.1. The maximum vertical displacement due to eruptions at E1S ranges from 0.1 to 20.6 $\mu$m. For the stacked data, the maximum displacement at E1S is 1.6 $\mu$m, so the stacked data represents a high

| Station | LVA | CON | E1S | NOE | UHT | NKB | HEL | HUT |
|---|---|---|---|---|---|---|---|---|
| Number of Events | 42 | 71 | 37 | 15 | 35 | 16 | 62 | 15 |

Table 2.1: Station name and the number of events used to gain stacked signals with high signal-to-noise ratios.

signal-to-noise, small magnitude eruption.

The signals are long duration, with the coda still being distinguishable past 200 seconds. However, due to limitations from computer memory, the inversion will only be performed on the initial 60 s of signal. Therefore, any evolution of the source process that might occur with time well into the coda will not be seen. The initial processes of the eruption and recharge phase will be modeled.

The inversion of the stacked data should give a reliable representative mechanism for the first 60 s of VLP coda because of its low noise. In particular, stacking events dramatically reduces the strong microseismic noise in the 7-14 s period band. It will not give information about the first few seconds of the signal which determines if an eruption is categorized as a Group 1 (positive initial vertical polarity) or Group 2 (negative initial vertical polarity) event. To gain information about the differences in the two different event types, an inversion will be done for an example of each of these as well. These inversions will involve more noise and thus may not be as reliable.

Ninety events were recorded during the 1999 field season [Mah, 2003]. An event on December 10, 1999 was chosen for the representative Group 1 inversion based on the high signal-to-noise ratio and because all of the stations were running at that time. Some components on some stations were drowned in noise and have been left out of the inversion, leaving a total of 17 seismograms.

The type of VLP signals slowly changed from dominantly Group 1 to Group 2 (negative first motions) from 1999 to 2002 [Mah, 2003]. Unfortunately, most of the clear Group 2 events happened in the mid-months of 2002 and often E1S was the only broadband seismometer running at that time. The activity at Erebus has gradually decreased since 2001 and this has also inhibited attempts at finding an especially good example of a negative polarity event with sufficient broadband coverage. An event on January 16, 2000 has a clear negative first motion and was chosen for the representative inversion for this event type. The vertical components have good signal-to-noise ratios for the 5 stations running at the time. However, some horizontal components were too noisy or not working properly and have been left out. The inversion is thus done on a total of 10 seismograms. Due to the decreased station coverage, and lack of much data from the tangential component, the results from this inversion are not expected to be as reliable as the other two inversions. However, it should still allow us to usefully contrast the general characteristics of the source mechanisms for the two styles of events. Also, with so few traces for the negative polarity event, a full inversion with six moment tensors and a single force is not suitably constrained. Fewer parameters must be used in the inversion in this case, using only three volumetric moment tensors and a vertical single force. As discussed later, this inversion will still give a valuable representation of the source mechanism.

# CHAPTER 3

## Methods

The general convolution equation to describe a seismogram is [Lay and Wallace, 1995]

$$u(t) = s(t) * g(t) * i(t) \tag{3.1}$$

where $*$ denotes convolution, $u(t)$ is the seismogram, $s(t)$ is the moment rate function, $g(t)$ is the Green's function that represents the Earth responses to a single-force or force-couple impulses, and $i(t)$ is the instrument response. Each moment tensor element corresponds to a particular Green's function. $g(t)$ also may include attenuation or other propagation effects. For this study, attenuation can be ignored because the seismic stations are within the near-field range of the source. Because the stations are a shorter distance than one wavelength (distances range from 0.7-2.5 km and the shortest wavelength for a period of 5 s and shear wave velocity of 1.27 km/s is 6.4 km), the waves will not be affected by small heterogeneities and so multipathing propagation effects are also ignored. Instrument impulse response is a known response that can be easily modeled given the type of seismometer. $s(t)$ is the unknown moment rate function for each of the Green's functions. In this application, the shape of $s(t)$ is expected to resemble, to some extent, the observed seismograms, because all of the stations are in the near-field of the source and the duration of the (impulsive source) Green's functions is relatively short compared to the signal duration.

The proportion of moment tensors as dictated by the moment rate functions (Figure 3.1) should tell us valuable information about the eruptive process. Earthquakes are often well described by double couple sources. As earthquake sources have a shearing motion and little to no volume change, their moment tensors are dominated by the deviatoric components. Thus, when modeling earthquakes, there is often a constraint of zero volume change (zero trace in the moment tensor elements). From Figure 3.1 it is seen that the tensor elements along the diagonal of the figure control volumetric changes and the off-diagonal (deviatoric) tensor elements control shear motions. This figure also illustrates the reason for the symmetry of the moment tensor. The figure for the (1,2) tensor element shows that these forces would lead to a clockwise rotation about the 3 axis. This force must be balanced. The (2,1) tensor element would cause a counterclockwise rotation about the 3 axis. Therefore, these forces must be equal if the source conserves angular momentum. A similar argument shows that the (1,3) tensor element equals the (3,1) and the (2,3) equals the (3,2). Therefore, the tensor is symmetric and only 6 elements are needed to describe the superposition of the force couples at a particular time.

For typical earthquake sources, six moment tensor elements considered can be reduced to 5 if it is assumed that there is no volume change, and this can be reduced to just three in the case of a planar fault [Lay and Wallace, 1995]. However, for volcanic settings, a change in volume is usually required, because volcanic processes involve expanding gases and motion of magma, which po-

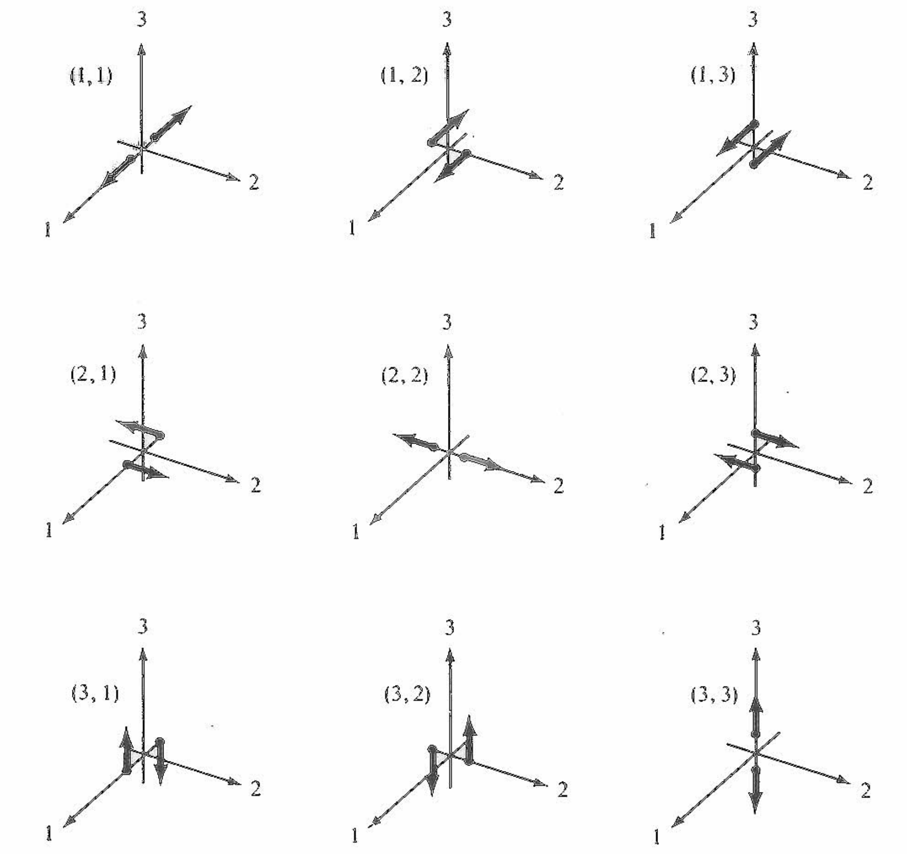

Figure 3.1: The nine moment tensor force couples. After (Aki and Richards, 2002).

tentially necessitates inverting for all six double couple forces.

The signals seen at Erebus are due to implosive or explosive forces associated with the buoyant transport and decompression of a bubble of gas within a magma conduit and to subsequent mass transport during lava lake refilling. Therefore, volumetric forces are likely to dominate the moment rate tensor solutions at Erebus, so that diagonal elements should be much larger than off-diagonal elements. Also, due to the movement and eruption of material, there may be forces that are not balanced internally by the Earth around them in the frequency band observed here. Instead of just the force couple mechanism represented in Figure 3.1, where every force is part of a force couple, there could also be single forces present (e.g. [Kanamori et al., 1984], [Chouet et al., 2003], [Ohminato et al., 1998]).

To find the moment rate function, the basic forward problem is to calculate synthetic seismograms based on a model and see how well they fit the observed seismograms. Inverse methods are used to iteratively solve for the model by minimizing the 2-norm of the residual.

A homogeneous half space with flat topography is used to calculate the Green's functions [Johnson, 1974]. Based on work from Dibble et al. [1994], a P-wave velocity of 2.2 km/s, an S-wave velocity of 1.27 km/s and a density of 2.4 g/cm$^3$ is assumed to characterize the bulk properties of the summit region. The program supplied by Johnson that calculates the Green's functions does so for a step-function and so the output of forward calculations must be differentiated to get an appropriate impulse response. It is easiest in practice to differentiate after the Green's functions and the moment rate function have been convolved together, as this minimizes instabilities arising from differentiating Green's functions that contain discontinuities.

The inversion for the moment rate function can be cast into a form involving k moment rate functions $m_i s_i(t)$ using

$$u_n(t) = i(t) * \sum_{i=1}^{k} m_i s_i(t) * G_{in}(t) \tag{3.2}$$

where the sum, k, is over each moment tensor element [Lay and Wallace, 1995]. n specifies the radial, tangential or vertical component. $G_{in}(t)$ is the Green's function corresponding to each moment tensor element for each component. The source can include up to six double couples and three single forces, for a total of nine moment tensor elements. $m_1 = M_{11}, m_2 = M_{12}, m_3 = M_{13}, m_4 = M_{22}, m_5 = M_{23}, m_6 = M_{33}, m_7 = F_1, m_8 = F_2, m_9 = F_3$. For the coordinate convention used in this paper, $x_1$ lies along the radial axis, which points to the lava lake, $x_2$ corresponds to the tangential axis, and $x_3$ is the vertical axis. The number of degrees of freedom necessary for a good fit is examined by modifying the allowable set of moment tensor elements. The models tested include only the volumetric double couple forces, the volumetric double couples plus a single vertical force, and all six double couple forces and the single vertical force.

Following Lay and Wallace [1995], an iterative inversion technique is applied to solve for the moment rate function. An initial synthetic seismogram is created using a starting model for the moment rate function. The starting model did not affect the results in this study, so a starting model composed of zeros was typically used. By iteratively updating the starting model to reduce the residual, or the difference between the observed and synthetic seismograms, a better model is achieved. The moment rate function is parameterized by a series of triangles of varying heights (Figure 3.2). Note that in our case, negative weight in the moment rate function is possible.

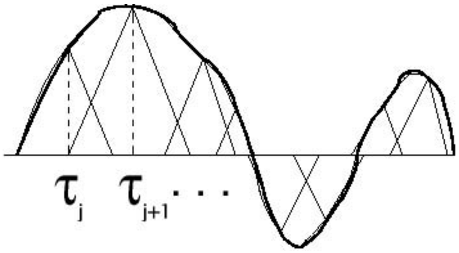

Figure 3.2: Source time function discretized as a series of triangles. Smooth curve is the superposition of the triangle functions.

Equation 3.2, for a particular seismogram component, is then rewritten as

$$u_n = i(t) * \sum_{j=1}^{M} \sum_{i=1}^{k} B_{ji}[b(t - \tau_j) * G_{in}(t)] \tag{3.3}$$

where $u_n$ is the seismogram, M is the number of triangle functions in the moment rate function characterization, $B_{ji}$ is the height of the jth triangle, and $b(t - \tau_j)$ is the triangle centered at time $\tau_j$. The duration and time spacing of the triangles (P samples) is an adjustable parameter, so the unknown is now $B_{ji}$. The initial starting model is now revised to minimize the residual. This is achieved by solving the following equation for $\mathbf{\Delta P}$

$$\mathbf{\Delta d} = \mathbf{A \Delta P} \tag{3.4}$$

where $\mathbf{\Delta d}$ is the residual between all observed and theoretical seismograms, $\mathbf{A}$ is a Jacobian matrix of partial derivatives and $\mathbf{\Delta P}$ is a vector of changes necessary in $B_{ji}$ to minimize $\mathbf{\Delta d}$. $\mathbf{A}$ is a matrix which contains information about the instrument response and Green's functions. **A** is calculated as the predicted response from a given source location at every sample interval.

$\mathbf{\Delta P}$ is then added to $B_{ji}$ to get the new starting model for the moment rate function. The process is now repeated with the new starting model. This continues until it converges. The shape of the moment rate function is able to vary for each moment tensor element considered. The results of the inversion were performed for 60 seconds of data at a sampling rate of 40 samples per second. To reduce wrap around effects caused by the Fourier Transform-calculated convolutions, the data are padded with zeros. The total number of sample points for each trace is thus 9216. For the stacked data, 24 traces are available. The number of triangles used to parameterize the moment rate function is 140. To reduce the size of the matrices, the seismograms are correspondingly filtered and decimated by a factor of 8 to a sample rate of 5 samples per second. The size of the **A** matrix is then (the number of traces (24) times the number of samples in each trace (1152)) 27648 by 140 times the number of moment tensor elements used.

The volumetric tensor elements dominate the source mechanisms recovered for VLP signals from Erebus. The ratio of the volumetric tensor elements reflects upon the type of volumetric expansion or dilatation occurring. A ratio of [1:1:1] means that the source volume is changing isotropically in all directions. If one of the components is larger than the others, this is similar to a volumetric source that is elongated in that direction. The implications of these ratios are covered further in the Discussion section.

To test the inversion technique, synthetic seismograms were generated to determine if the moment rate function can be successfully recovered. Synthetics were created for the eight stations with three components used in the inversion of the stacked data. Various source models were tested, including a purely volumetric source, a volumetric source plus a single force, and all six force couples plus a single force. The moment rate function was recovered adequately for all combinations that were run after about three iterations. The fit of synthetics waveforms to the observed waveforms was computed with equation 3.5.

$$\text{variance reduction} = \frac{\sum_{i=1}^{N} u_i^{o2} - \sum_{i=1}^{N} (u_i^o - u_i^s)^2}{\sum_{i=1}^{N} u_i^{o2}} \times 100\% \qquad (3.5)$$

where $u^o$ is the data trace, $u^s$ is the synthetic trace, and $N$ is the number of samples in each trace.

Figure 3.3 shows the fit to the synthetics and to the moment rate function for a Mogi source; a model that is a spherical body, such as a magma chamber, at depth, that contracts and expands due to changing internal pressure. This isotropic source has been widely used as a first-order model for the deformation seen at some volcanoes during eruptions or magma chamber inflation [Mogi, 1958]. Figures 3.4 and 3.5 show the tests for a source with all six components and a vertical force. Figures 3.3 and 3.4 show models which did not include noise.

The inversion process is tested using the signal from CON as the source time function for the force couples in this case to check that it would

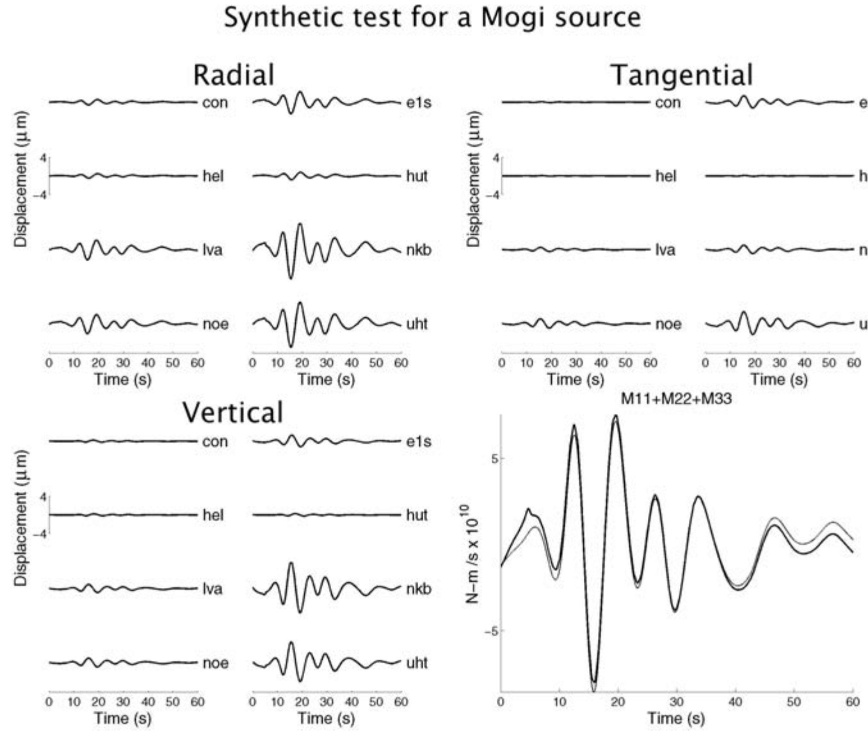

Figure 3.3: Synthetic seismograms and the modeled fit for a Mogi source ($M_{11} = M_{22} = M_{33}$). The solid lines are the true model, the thin lines are the inverse solution. The fit of the seismograms is sufficiently exact that the traces overlay almost exactly. a) radial component. b) tangential component. c) vertical component. d) the moment rate function.

invert stably for signals with the long periods and long durations such as probably exist for the true source.

Tests were also performed to determine the effect that a source mislocation would have on the recovered source mechanism. Mislocations by 100 m in the vertical direction and by 20 m in the north-south and east-west directions were investigated. The source mechanism for the synthetic seismograms was a crack model with a [1:1:3] moment tensor element ratio (Figure 3.6).

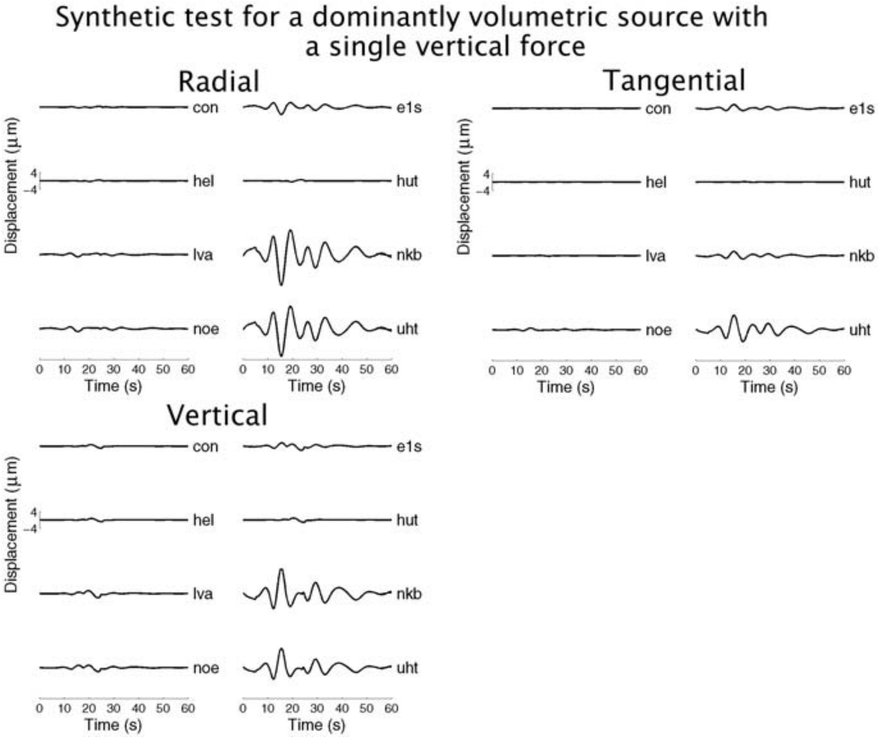

Figure 3.4: Synthetic seismograms and the modeled fit for a dominantly volumetric source with a ratio of [1:1:3] and a vertical single force (shown in Figure 3.5). The solid lines are the true data, the thin lines are the inverse solution. a) radial component. b) tangential component. c) vertical component. The fit is sufficiently exact that the traces overlay almost exactly.

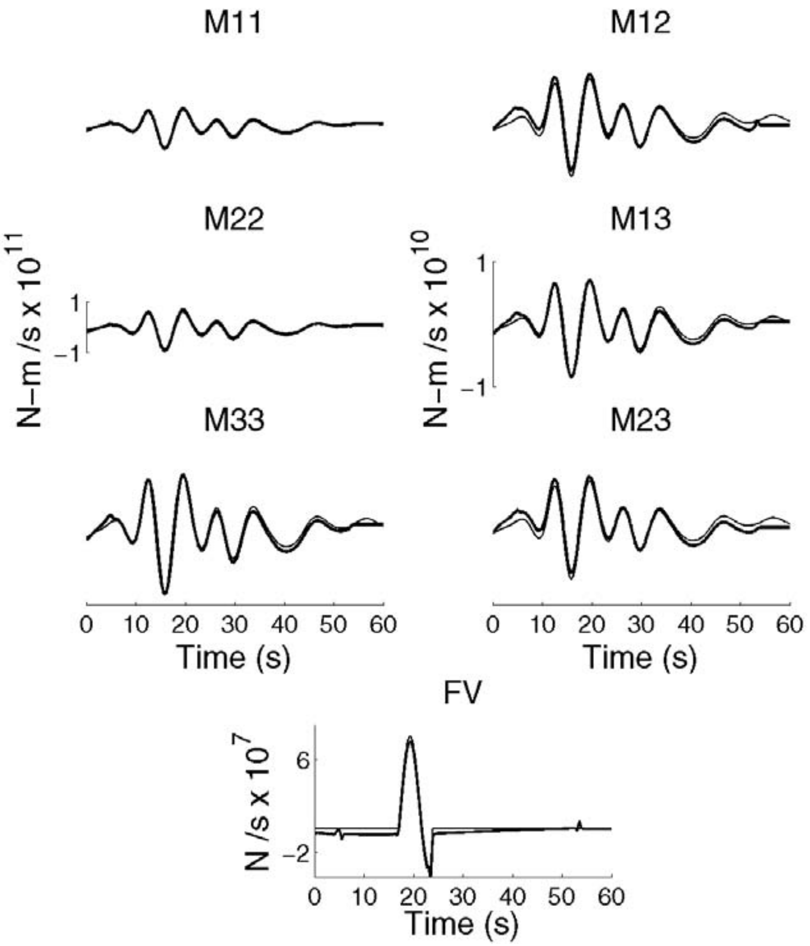

Figure 3.5: Moment rate function for seismograms in Figure 3.4, a dominantly volumetric source plus a single vertical force. The thick lines are modeled and the thin lines are synthetic. $F_v$ is the single vertical force.

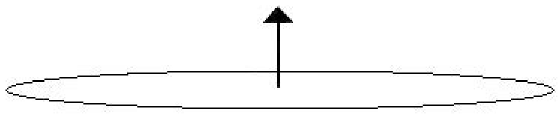

Figure 3.6: Inflating subhorizontal crack model in a Poisson solid corresponding to a theoretical [1:1:3] moment tensor element ratio.

For all mislocations, the volumetric tensor elements have smaller errors than the deviatoric elements. The non-diagonal tensor elements are of smaller amplitude and so are greater affected by a source mislocation since the inversion program will preferentially fit the elements with a larger amplitude. The single force consistently has small oscillations introduced into the pulse-like waveform. When the modeled source location is 100 meters deeper than the actual source, the volumetric tensor elements are still closely matched with variance reductions of 93-97% (Figure 3.7). The $M_{13}$ and $M_{23}$ tensor elements still have the appropriate waveform but are overestimated and have variance reductions of 96% and 63% respectively. The $M_{12}$ component is not matched. The single force is overestimated and has a variance reduction of 88%. The $M_{11}$ and $M_{22}$ tensor elements are overestimated, so a source mislocation of 100 meters deeper than the actual source would cause the mechanism to look less like a crack and more like an isotropic source. The modeled ratio of the diagonal moment tensor elements is [1.1:1.3:3]. When the modeled source location is 100 meters shallower than the actual source (Figure 3.8), the couples are consistently overestimated except the $M_{23}$ tensor element which is underestimated and the waveforms do not match. The variance reduction for the other elements ranges from 74-89%. The single force is underestimated and has a variance reduction of 88%. The volumetric ratio is [1:0.9:3]. When the source is offset 20 meters to the west, the moment tensor elements are underestimated (Figure 3.9). The $M_{13}$ tensor element does not match the waveform. The other couples have variance reductions ranging from 56-96%. The single force is underestimated and has a variance reduction of 95%. The volumetric ratio is [1.1:1.1:3]. When the source is offset 20 meters to the east, the couples are consistently overestimated but the single force is underestimated (Figure 3.10). The volumetric tensor elements have variance reductions ranging from 94-97%. The deviatoric tensor elements have variance reductions ranging from 59-92%. The single force has a variance reduction of 97%. The volumetric ratio is [0.9:1:3]. When the source is offset 20 meters north, the volumetric tensor elements have variance reductions ranging from 93-96% (Figure 3.11). The $M_{12}$ tensor element does not match the waveform at all and the $M_{13}$ and $M_{23}$ tensor elements have variance reductions of 54% and 93% respectively. The single force has a variance reduction of 96%. The $M_{11}$ and $M_{22}$ tensor elements are overestimated while the $M_{33}$ tensor element is underestimated. This makes the source look more isotropic with a volumetric ratio of [1.2:1.4:3]. When the source is offset 20 m south, the $M_{13}$ tensor element does not match the waveform (Figure 3.12). The volumetric tensor elements have variance reductions ranging from 96-97% and the $M_{12}$ and $M_{23}$ tensor elements have variance reductions of 68% and 86% respectively. The single force is underestimated and has a variance reduction of 93%. The volumetric tensor ratio is [1:1.1:3].

Overall, the volumetric ratios were significantly affected by source mislocations, but the general moment rate function was still recovered. The ratio remains approximately [1:1:3] and the off-diagonal components remain small. A source mislocation to the north has the largest effect on the volumetric ratio.

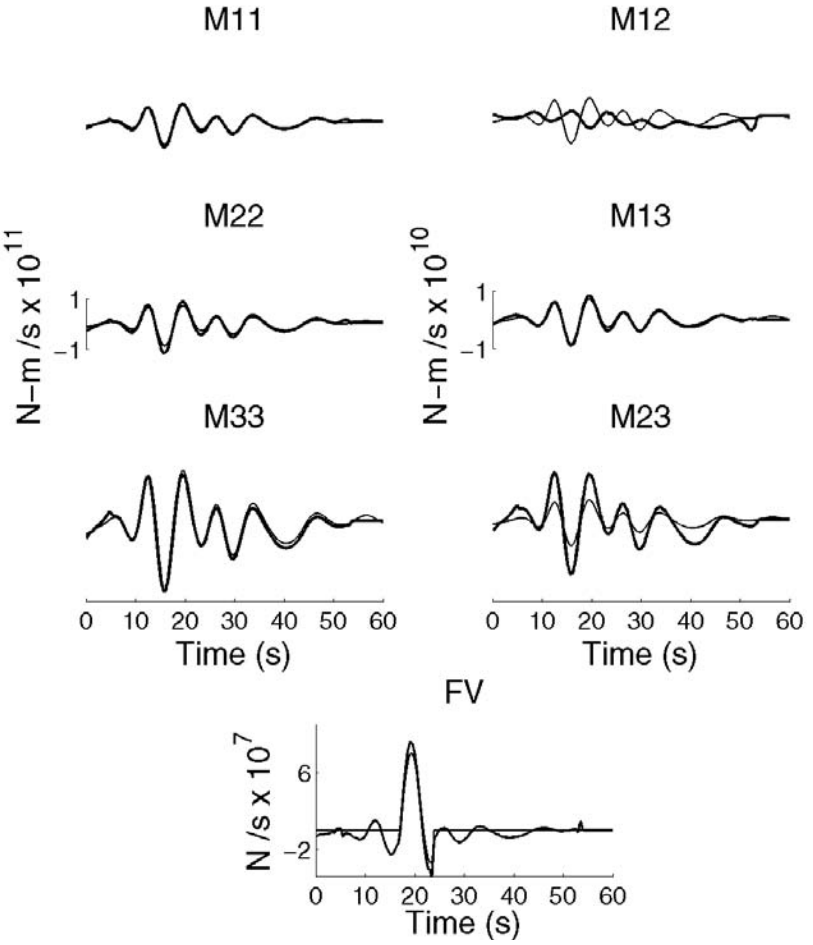

Figure 3.7: Synthetics showing results on source mechanism for a source mislocation. The thicker lines are modeled and the thinner lines are synthetic. Source mislocation is a source offset 100 meters deeper than the actual source. Note the different scales for the volumetric and deviatoric tensor elements.

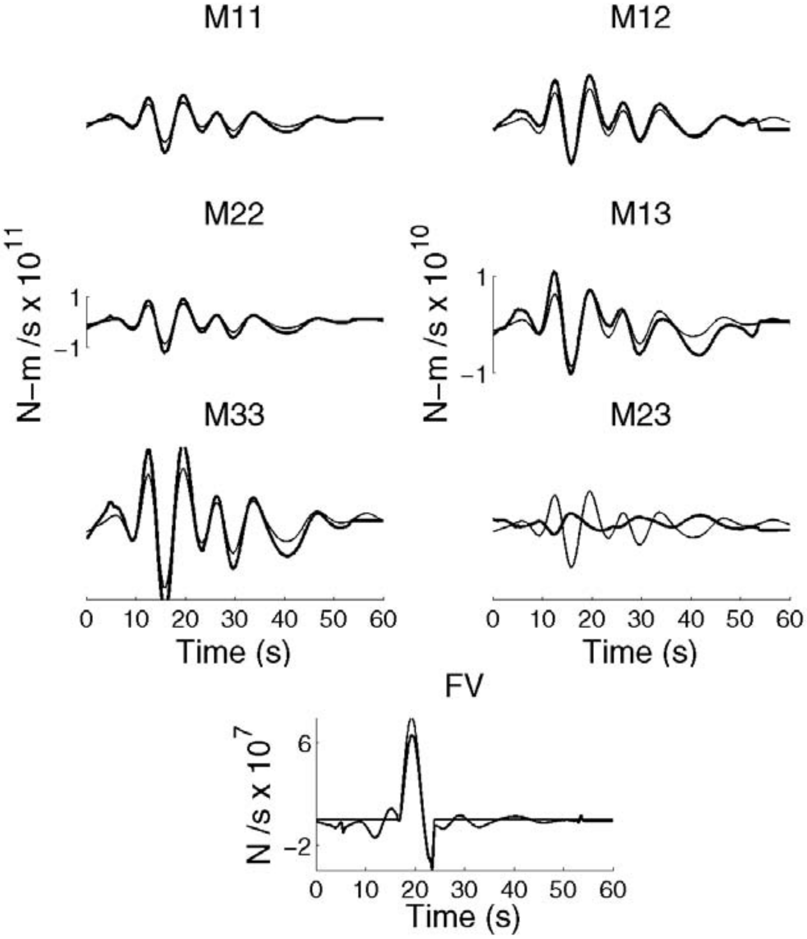

Figure 3.8: Synthetics showing results on source mechanism for a source mislocation. The thicker lines are modeled and the thinner lines are synthetic. Source mislocation is a source offset 100 meters shallower than the actual source. Note the different scales for the volumetric and deviatoric tensor elements.

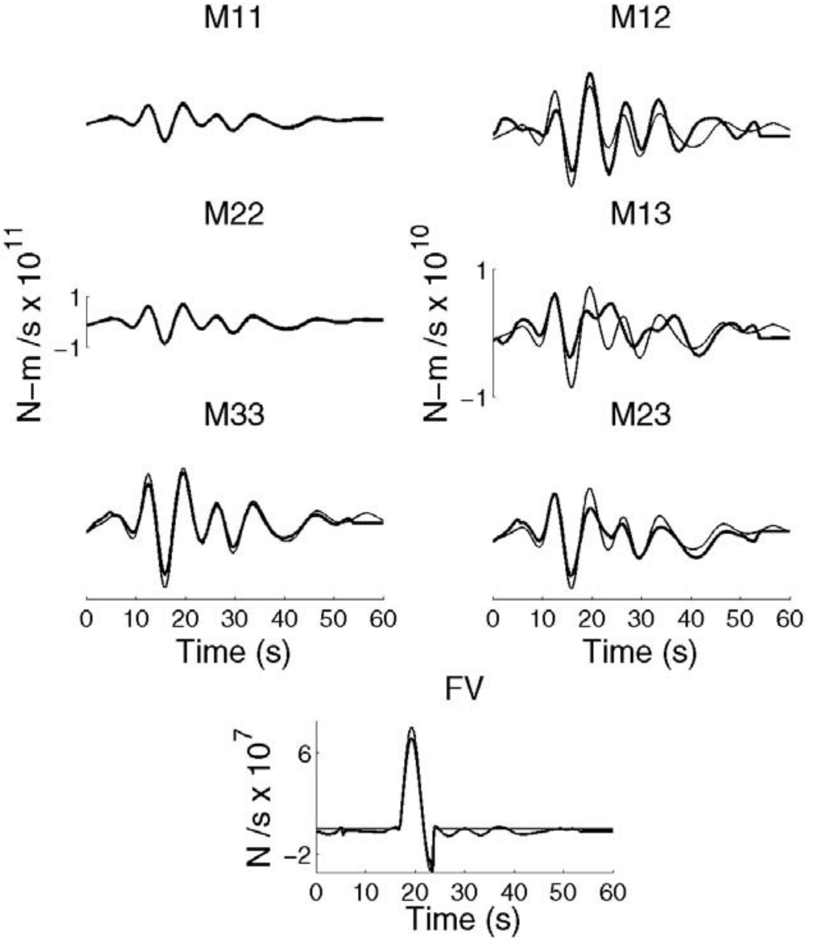

Figure 3.9: Synthetics showing results on source mechanism for a source mislocation. The thicker lines are modeled and the thinner lines are synthetic. Source mislocation is a source offset 20 meters to the west of the actual source. Note the different scales for the volumetric and deviatoric tensor elements.

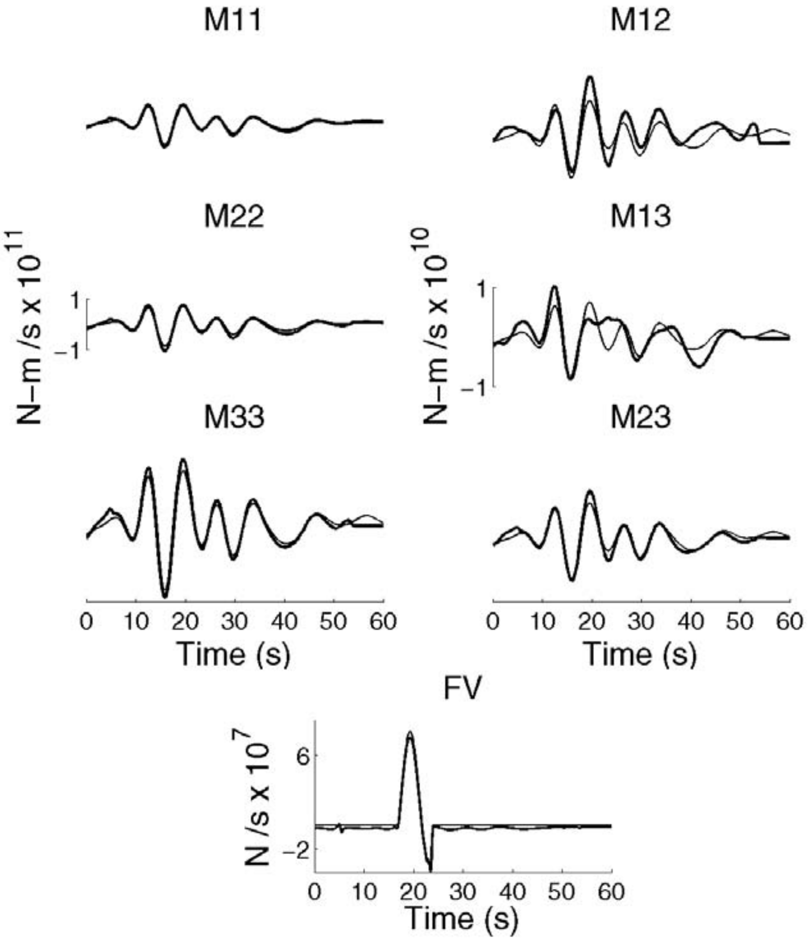

Figure 3.10: Synthetics showing results on source mechanism for a source mislocation. The thicker lines are modeled and the thinner lines are synthetic. Source mislocation is a source offset 20 meters to the east of the actual source. Note the different scales for the volumetric and deviatoric tensor elements.

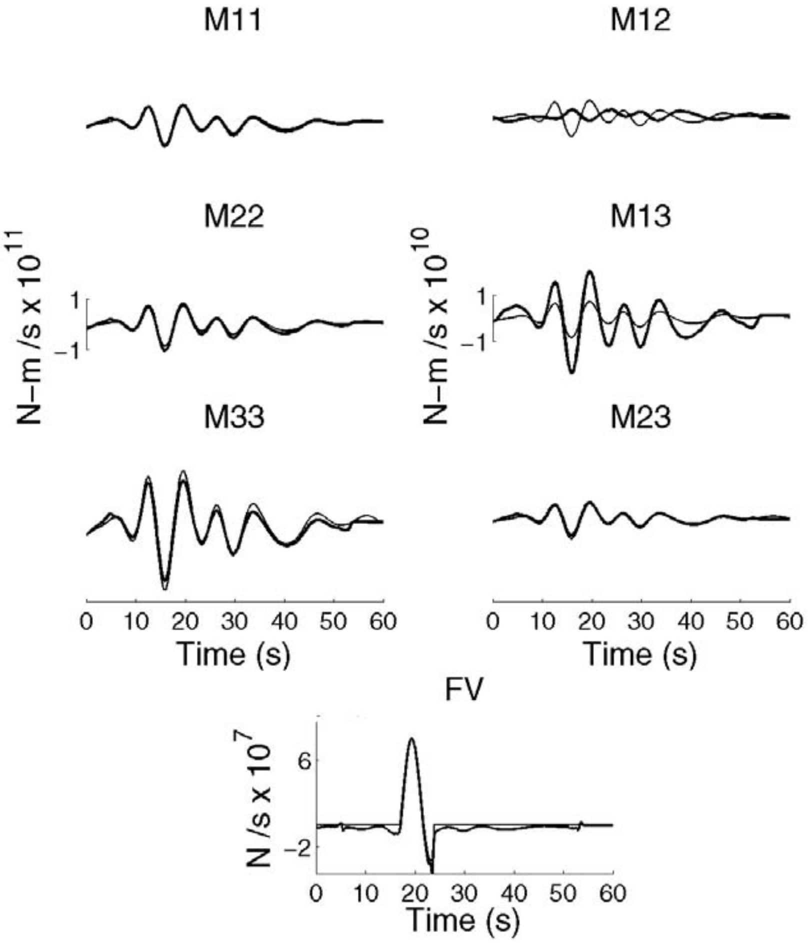

Figure 3.11: Synthetics showing results on source mechanism for a source mislocation. The thicker lines are modeled and the thinner lines are synthetic. Source mislocation is a source offset 20 meters to the north of the actual source. Note the different scales for the volumetric and deviatoric tensor elements.

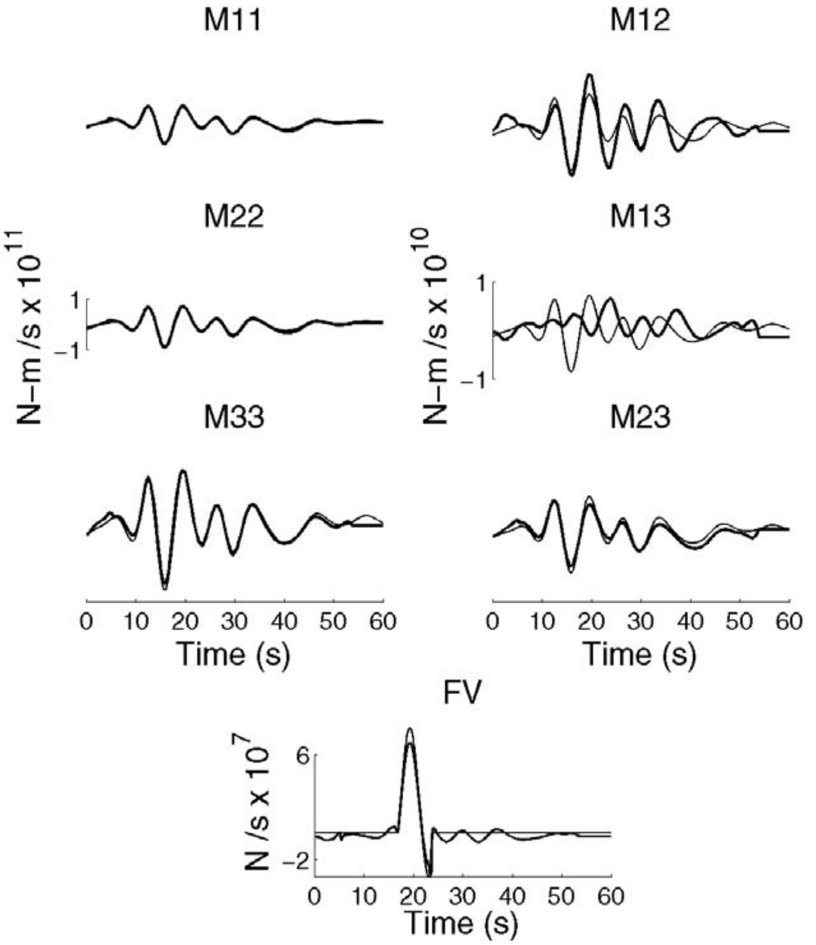

Figure 3.12: Synthetics showing results on source mechanism for a source mislocation. The thicker lines are modeled and the thinner lines are synthetic. Source mislocation is a source offset 20 meters south of the actual source. Note the different scales for the volumetric and deviatoric tensor elements.

# CHAPTER 4

# Results

Particle motion analysis can give a rough estimate of the source location [Mogi, 1958] and was used as a preliminary starting point for the search for the best location. A grid defines the area being considered as a possible source location. The inversion is performed for every source point located within a box (Figure 4.1) with spacings of 0.0032 degrees or about 350 meters and depths of 100, 200, and 300 meters. The spacing is subsequently decreased to zoom in on the areas with the best fit. The smallest grid spacing with resolvable results is 0.0002 degrees latitude and 0.0008 degrees longitude or about 20 meters. Depths deeper than 300 meters give a slightly improved fit, however, they are considered to be unreliable because some nonvolumetric components are large and some volumetric components are small. Also, the value of the P-wave velocity used in the Green's functions calculations is only valid down to around 300-400 meters. There the velocity increases as the material turns to more compacted volcanics [Dibble et al., 1994]. However, the unreliability of deeper depths is also a non-issue because video observations of the lava lake and its evisceration clearly suggest a shallow VLP source process, perhaps limited to the uppermost 100 meters [Aster et al., 2003].

Increasing the number of allowed moment tensor elements predictably leads to an improvement in fit. The inversion was first done assuming only a

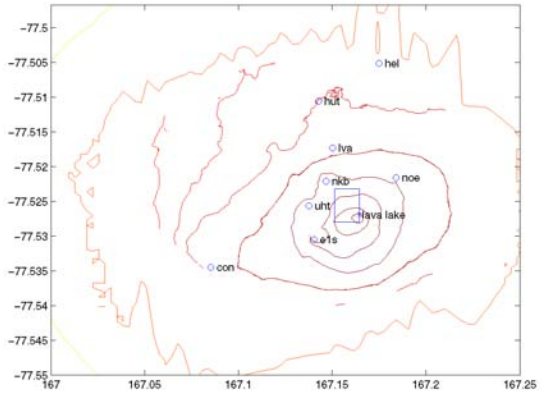

Figure 4.1: Topographic map of Erebus showing the box throughout which the best source location search was performed. The box is 100-300 m in depth.

single moment rate function with a fixed ratio of moment tensor volumetric elements. All of the following models for the stacked data have an assumed source location which is the same as the best fit source location found for the model which has all six moment tensors and a single vertical force. A purely Mogi source was first used, where the volumetric moment tensor elements have a ratio of [1:1:1] (Figure 4.2). This model is unable to match the majority of vertical and tangential seismograms, and features a variance reduction of only 17% for the vertical component and 21% for all of the traces.

Next, a single moment rate function model with a fixed diagonal moment tensor element ratio consistent with a horizontal crack was considered. Two ratios [1:1:2] and [1:1:3] were used (see Figure 4.3 and Figure 4.4). These models also did not provide especially good fits to the data. The crack with the [1:1:2] ratio has a better fit than the crack with the [1:1:3] ratio with variance reductions of 19% and 11% respectively, but still not as good a fit as the Mogi

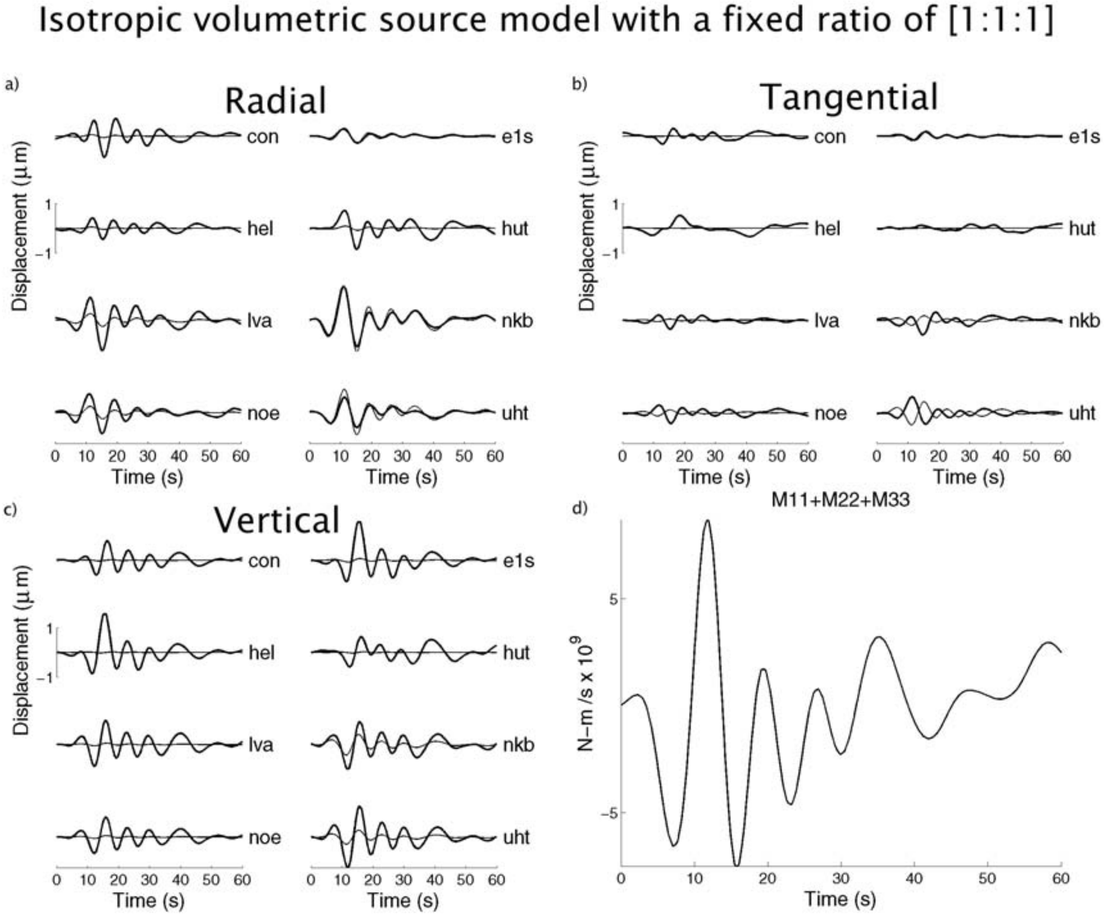

Figure 4.2: Results for a Mogi model with only volumetric components and an assumed moment tensor element ratio of [1:1:1]. The thick lines are the observed seismograms and the thin lines are the synthetic seismograms. Radial, tangential, and vertical component fit to the stacked data as characterized by variance reduction. a) the synthetics fit 50% of the observed radial component. b) the synthetics do not fit the observed tangential component. c) the synthetics fit 17% of the observed vertical component. d) the moment rate function.

source. This shows that a single purely volumetric moment rate function with set ratio is inadequate to fit the observed data.

To obtain a better fit to the data, it is therefore necessary to increase the degrees of freedom beyond that allowed by purely isotropic and volumetric (Mogi) sources, or simple subhorizontal crack-like models. The next model that we considered has the two tensor elements $M_{11}$ and $M_{22}$ fixed to be a 1:1 ratio, but the $M_{33}$ element is now free to have its own moment rate function. This model shows notable improvement and we are now starting to fit the vertical component significantly better, with a variance reduction of 27% for the vertical component (Figure 4.5). The ratio found for the maximum peak to trough amplitude of these moment tensor elements is [0.8:0.8:3]. Again, however, the overall fit is not especially good, with a total variance reduction of 28%.

Next, the moment rate function for each of the three volumetric components is allowed to vary with time (Figure 4.6). The approximate ratio in the solution found for the maximum peak to trough amplitude is [0.8:0.7:3]. This is similar to the previous result and since the ratio of the $M_{11}$ and $M_{22}$ components is close to 1:1, not much appears to have been gained from this increase in solution freedom. The variance reduction shows that 30% of the traces are now fit.

A further step in model complexity is to allow for nonvolumetric components. Results show, however, that required nonvolumetric components are small compared to the volumetric components (Figure 4.7). They increase the degree of fit, but the vertical component is still not being adequately modeled.

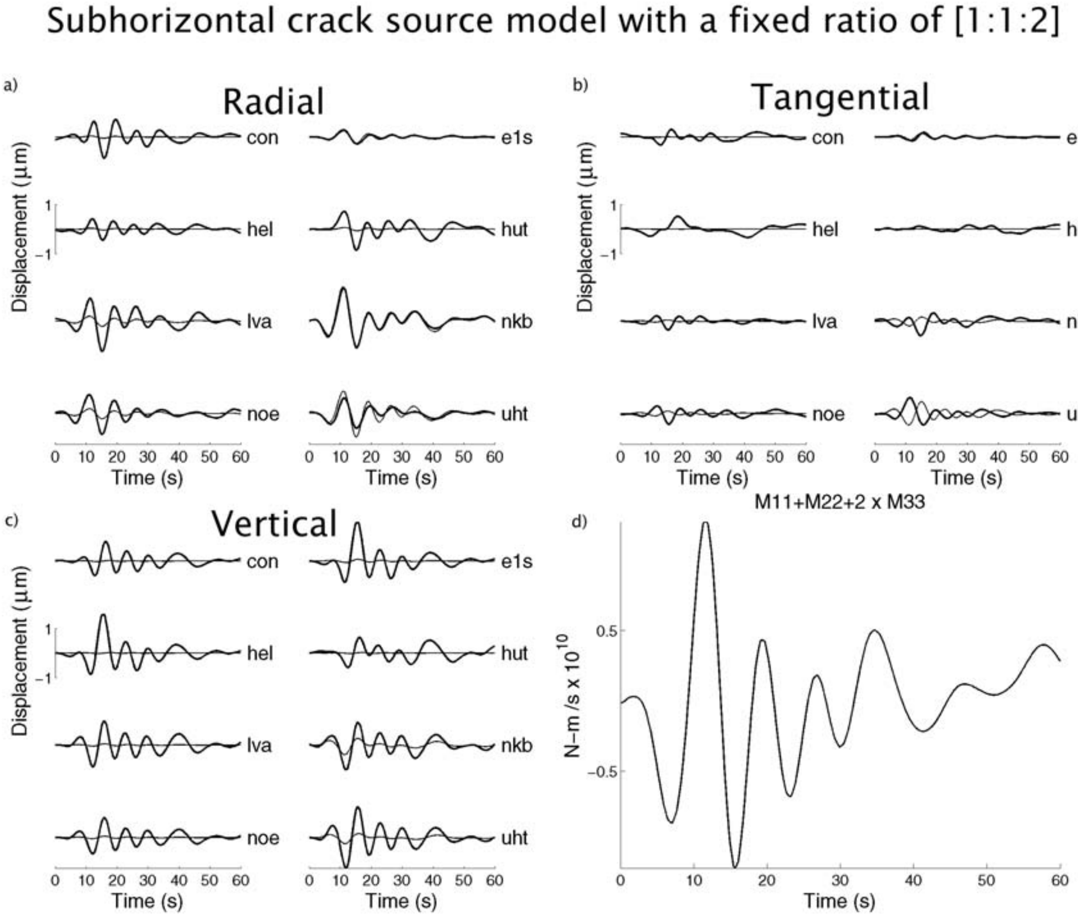

Figure 4.3: Results for a subhorizontal crack-like model with only volumetric components and an assumed moment tensor element ratio of [1:1:2]. The thick lines are the observed seismograms and the thin lines are the synthetic seismograms. Radial, tangential, and vertical component fit to the stacked data as characterized by variance reduction. a) the synthetics fit 47% of the observed radial component. b) the synthetics do not fit the observed tangential component. c) the synthetics fit 14% of the observed vertical component. d) the moment rate function.

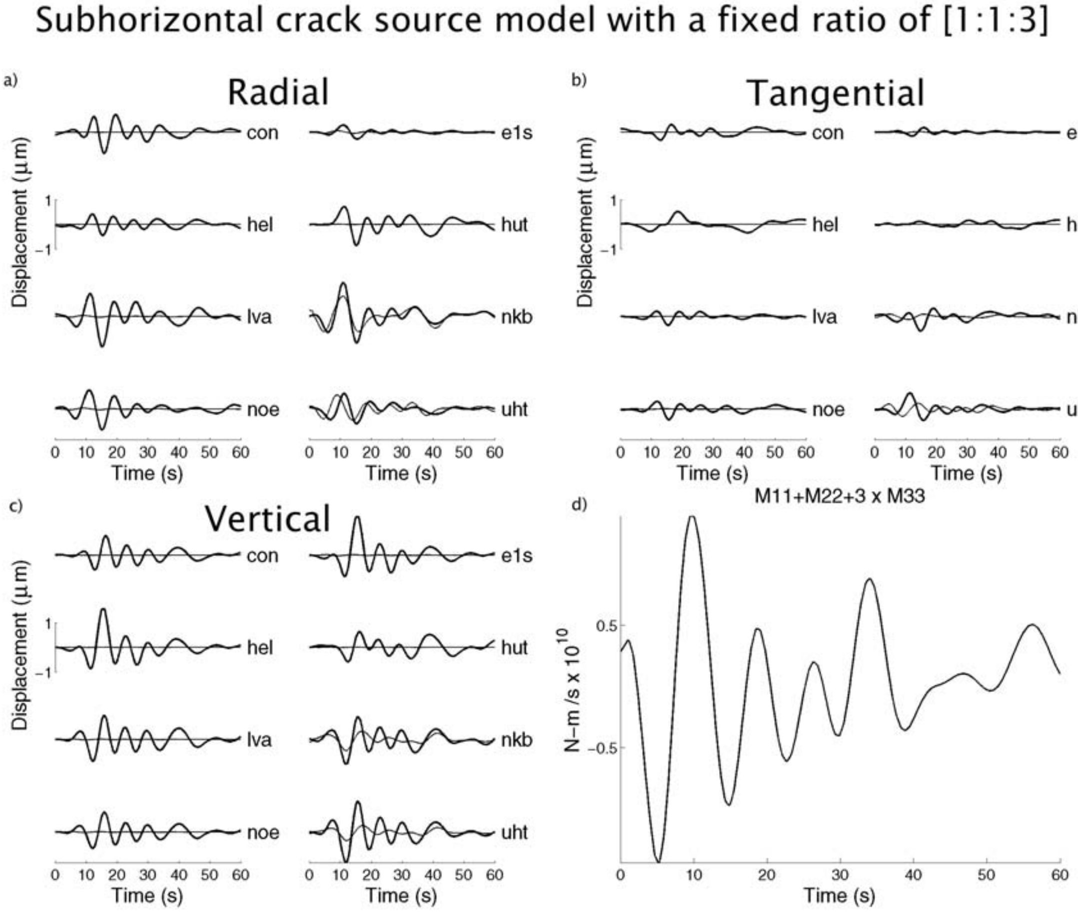

Figure 4.4: Results for a subhorizontal crack-like model with only volumetric components and an assumed moment tensor element ratio of [1:1:3]. The thick lines are the observed seismograms and the thin lines are the synthetic seismograms. Radial, tangential, and vertical component fit to the stacked data as characterized by variance reduction. a) the synthetics fit 19% of the observed radial component. b) the synthetics do not fit the observed tangential component. c) the synthetics fit 10% of the observed vertical component. d) the moment rate function.

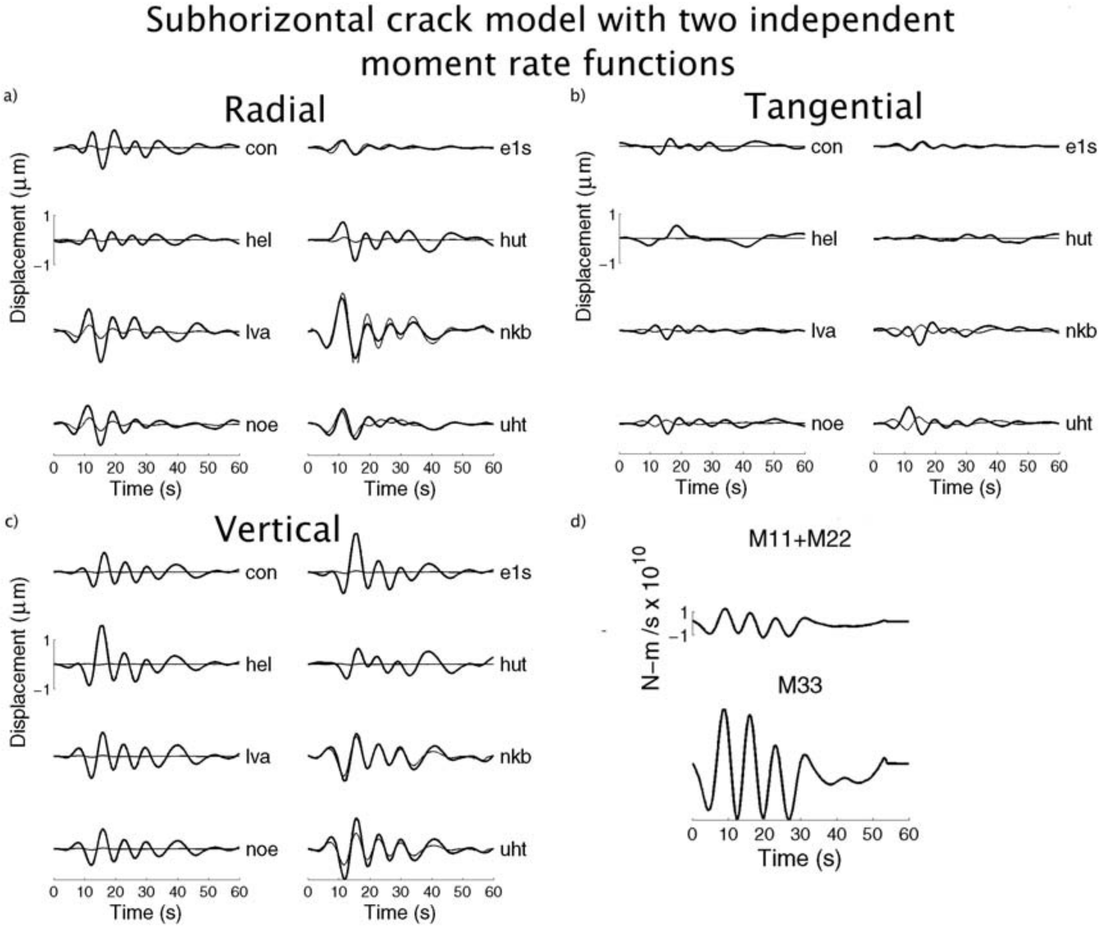

Figure 4.5: Results for a model with only volumetric components where the moment rate function of $M_{11}$ to $M_{22}$ is held to be equal, but $M_{33}$ can vary. Radial, tangential, and vertical component fit to the stacked data as characterized by variance reduction. a) the synthetics fit 46% of the observed radial component. b) the synthetics do not fit the observed tangential component. c) the synthetics fit 27% of the observed vertical component. d) the moment rate functions.

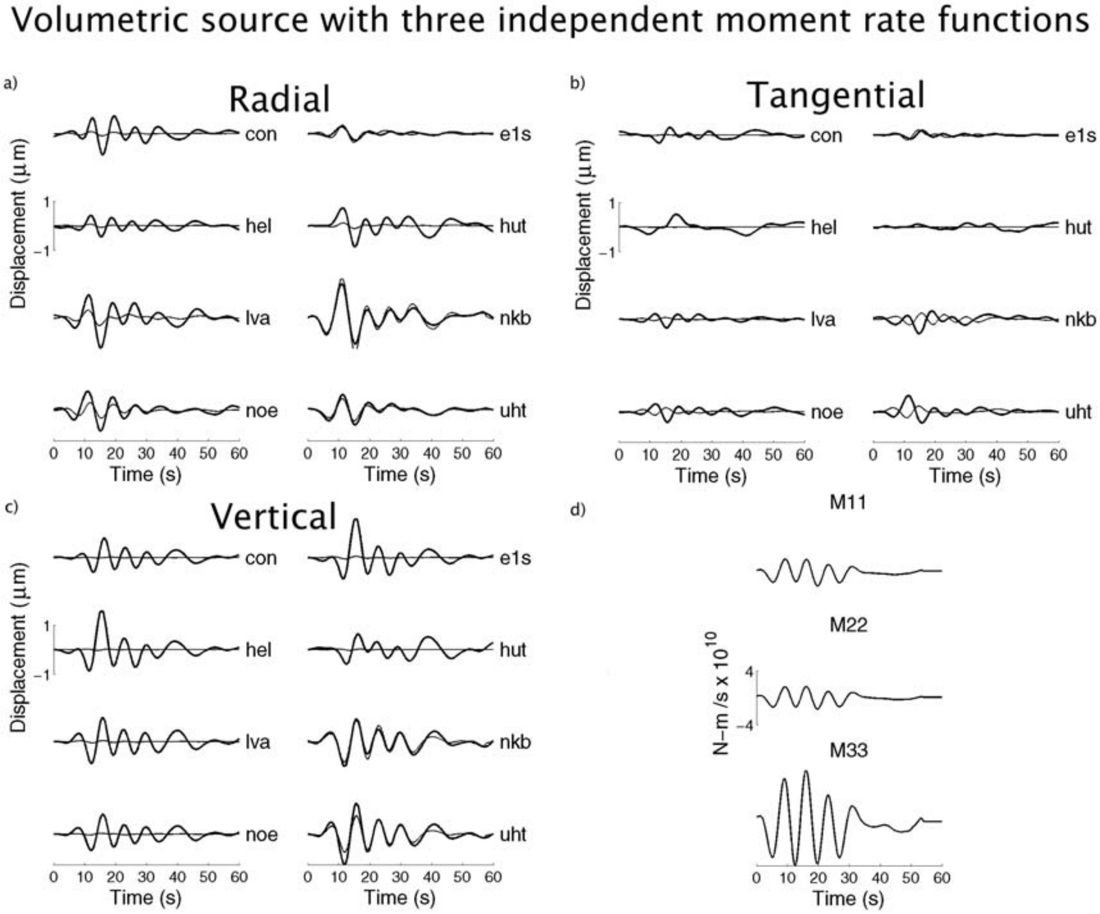

Figure 4.6: Results for a volumetric source where the moment rate functions of all three elements are free to vary. The thick lines are the observed seismograms and the thin lines are the synthetic seismograms. Radial, tangential, and vertical component fit to the stacked data as characterized by variance reduction. a) the synthetics fit 51% of the observed radial component. b) the synthetics do not fit the observed tangential component. c) the synthetics fit 29% of the observed vertical component. d) the moment rate functions.

The variance reduction for all of the components has increased to 47% but is still only 49% for the vertical component. The ratio found for the maximum peak to trough amplitude for the volumetric tensor elements is [0.8:0.8:2].

We next considered a model that has the six double couples, but also includes a single vertical force. Only now is the vertical component significantly fit with a variance reduction of 75% (Figure 4.8). The vertical single force is clearly necessary to the model (Figure 4.9). The total variance reduction for all of the traces is now 67%. The tangential component is never fit by any of the models. The amplitudes for tangential traces are smaller than the vertical and radial components and so the vertical and radial traces are preferentially fit. Since the energy represented on the tangential traces is small compared to the contribution of the radial and vertical traces, we feel that the inability to fit the tangential traces does not represent a significant problem with the best fit model. The volumetric components give a maximum peak to trough ratio of [1.1:1:3]. And again, the nonvolumetric components are much smaller than the volumetric ones (Table 4.3).

By inverting for a model which includes the three volumetric components and a single force, it can be shown that the single force is more important to fitting the data than the deviatoric components (Figure 4.11). This model with fewer parameters provides a better fit than inverting for the six moment tensors, again indicating the importance of the single vertical force (Figure 4.10). The total variance reduction for all the seismograms is 61%.

The model including the six couples and the single force is the best model, although the deviatoric elements only marginally improve the fit. This

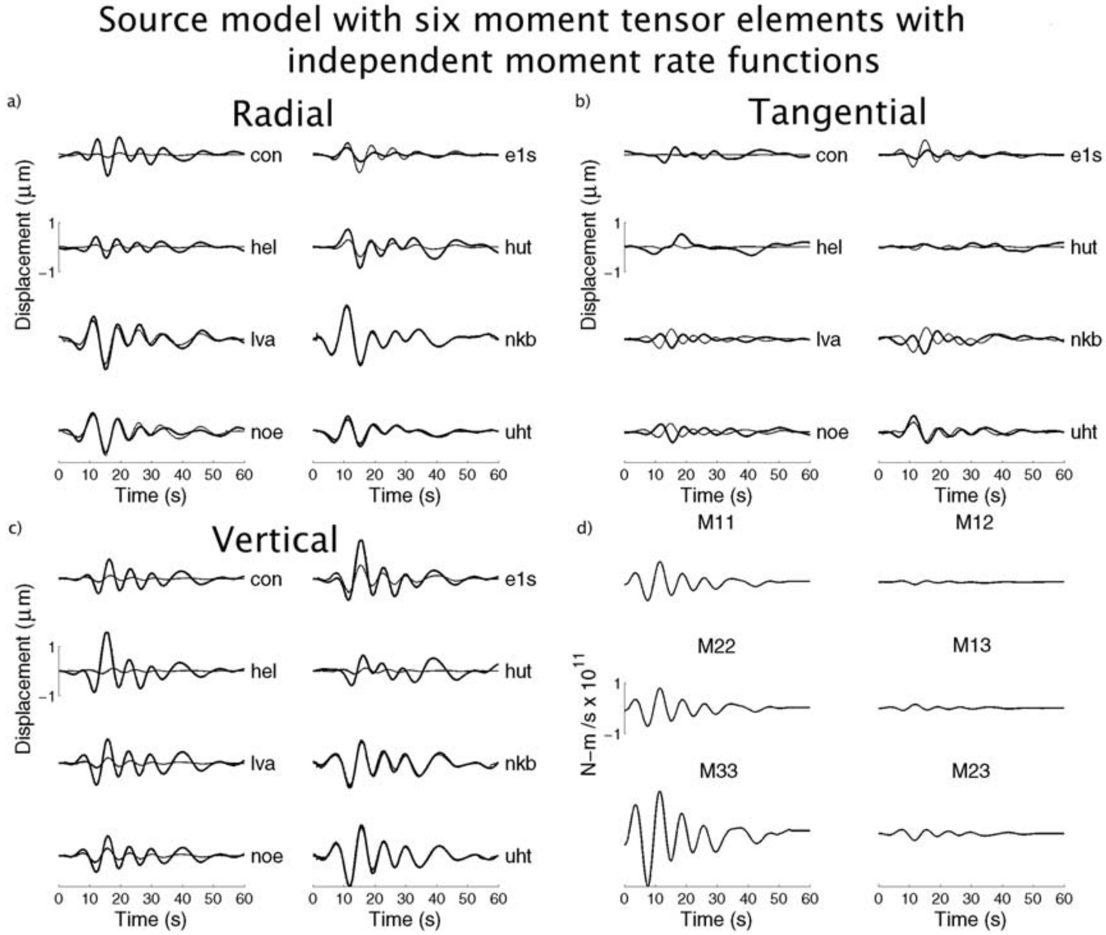

Figure 4.7: Results for a model with all six moment tensor elements and independent moment rate functions. The thick lines are the observed seismograms and the thin lines are the synthetic seismograms. Radial, tangential, and vertical component fit to the stacked data as characterized by variance reduction. a) the synthetics fit 73% of the observed radial component. b) the synthetics do not fit the observed tangential component. c) the synthetics fit 49% of the observed vertical component. d) the moment rate functions.

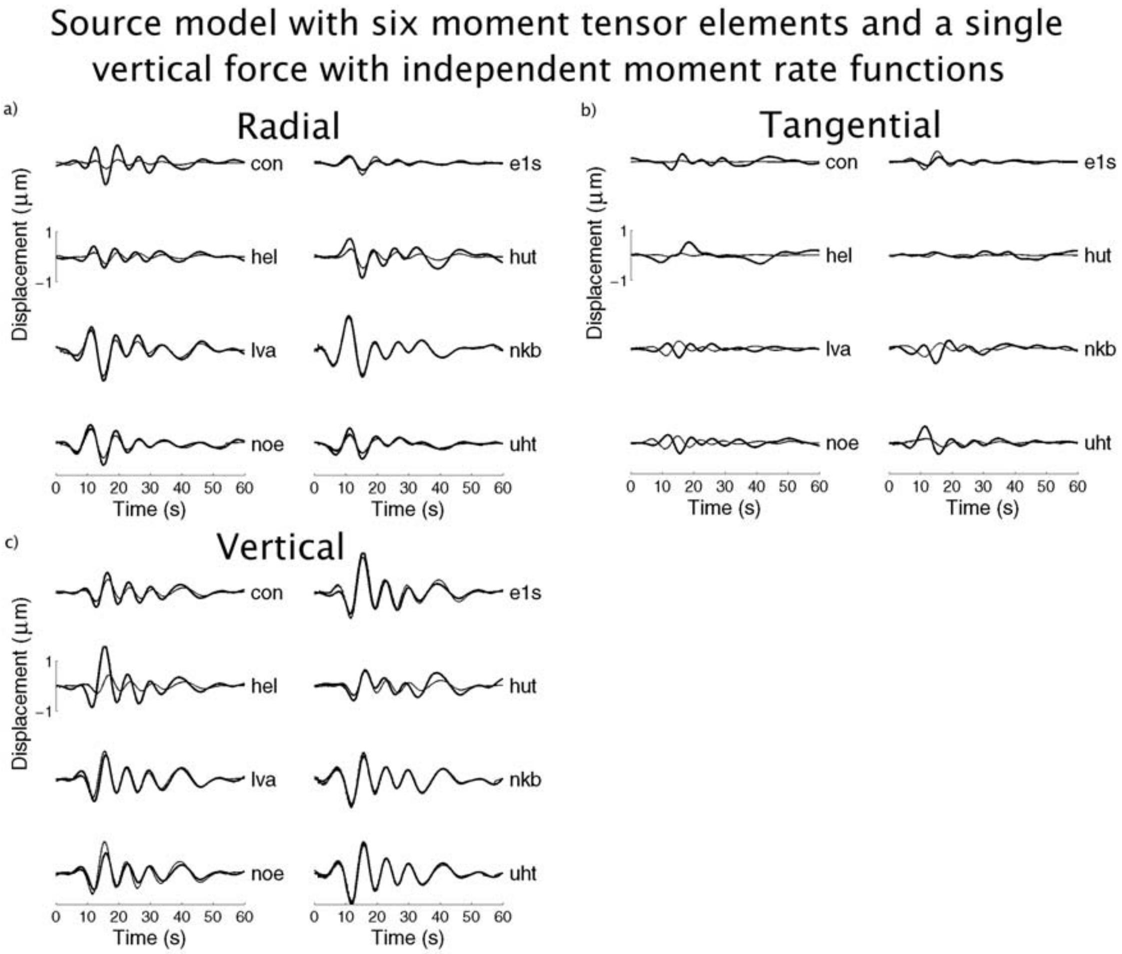

Figure 4.8: Results for a model with six independent moment tensor elements and moment rate functions and a vertical single force. Radial, tangential, and vertical component fit to the stacked data as characterized by variance reduction. The thick lines are the observed seismograms and the thin lines are the synthetic seismograms. a) the synthetics fit 79% of the observed radial component. b) the synthetics do not fit the observed tangential component. c) the synthetics fit 75% of the observed vertical component.

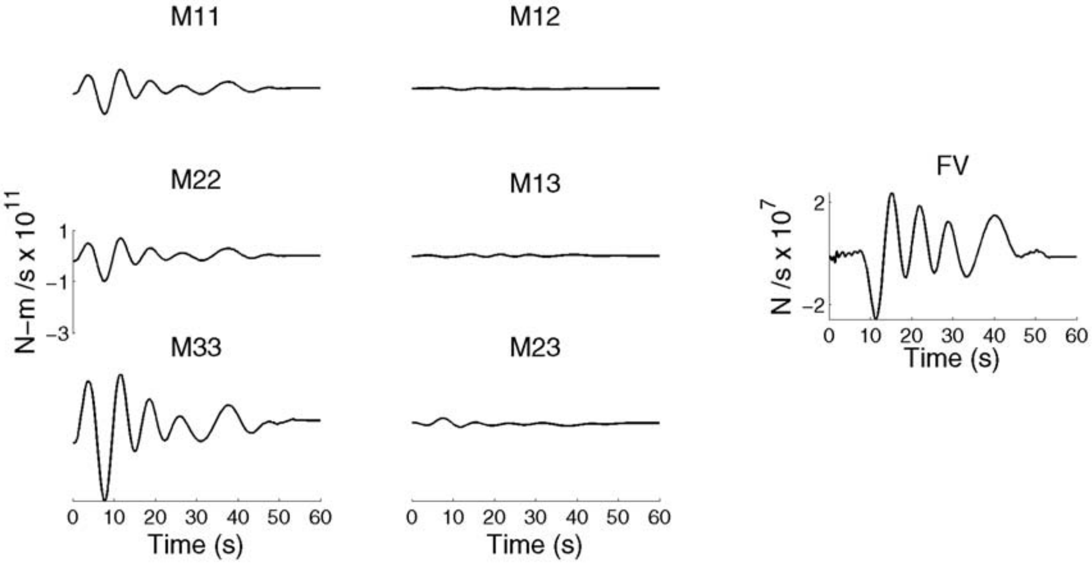

Figure 4.9: Moment rate functions corresponding to Figure 4.8. Note that the volumetric components are significantly larger than the deviatoric components.

model fits the observables with the highest variance reduction (Table 4.1). The models with volumetric elements but no single force show a larger relative amplitude for the $M_{33}$ tensor element compared to the $M_{11}$ and $M_{22}$ tensor elements than the models which include a single force. This shows that the $M_{33}$ tensor element attempts to compensate for the single force in the earlier models.

It must be determined if the increase in fit is simply due to an increase in the number of source parameters. The Akaike Information Criterion (AIC) takes the number of free parameters into account [Akaike, 1974].

$$AIC = N \log S + 2r \tag{4.1}$$

where $N$ is the number of samples in all the data traces, $S$ is the total variance reduction from equation (3.5), and $r$ is the number of free parameters. If the

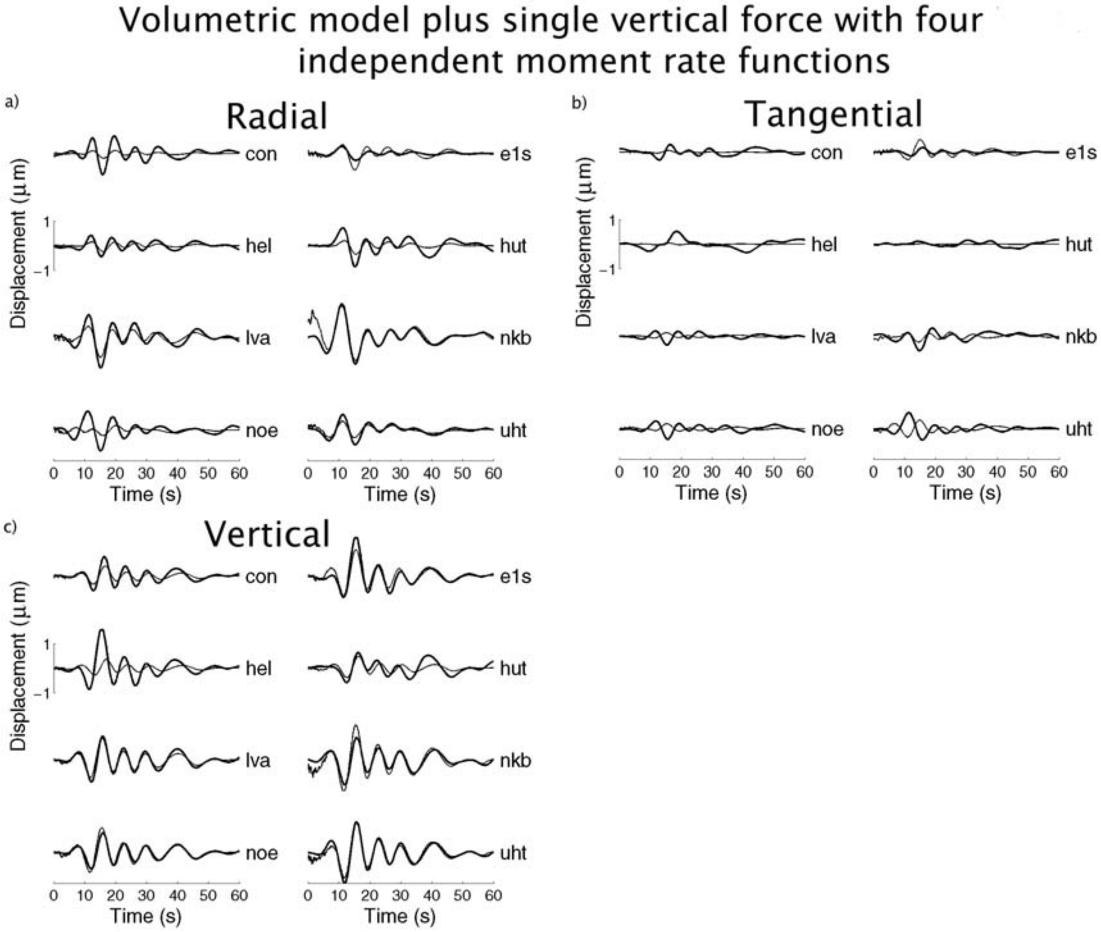

Figure 4.10: Results for a model with only the volumetric tensor elements and a single vertical force. The thick lines are the observed seismograms and the thin lines are the synthetic seismograms. Radial, tangential, and vertical component fit to the stacked data are characterized by variance reduction. a) the synthetics fit 54% of the observed radial component. b) the synthetics do not fit the observed tangential component. c) the synthetics fit 68% of the observed vertical component.

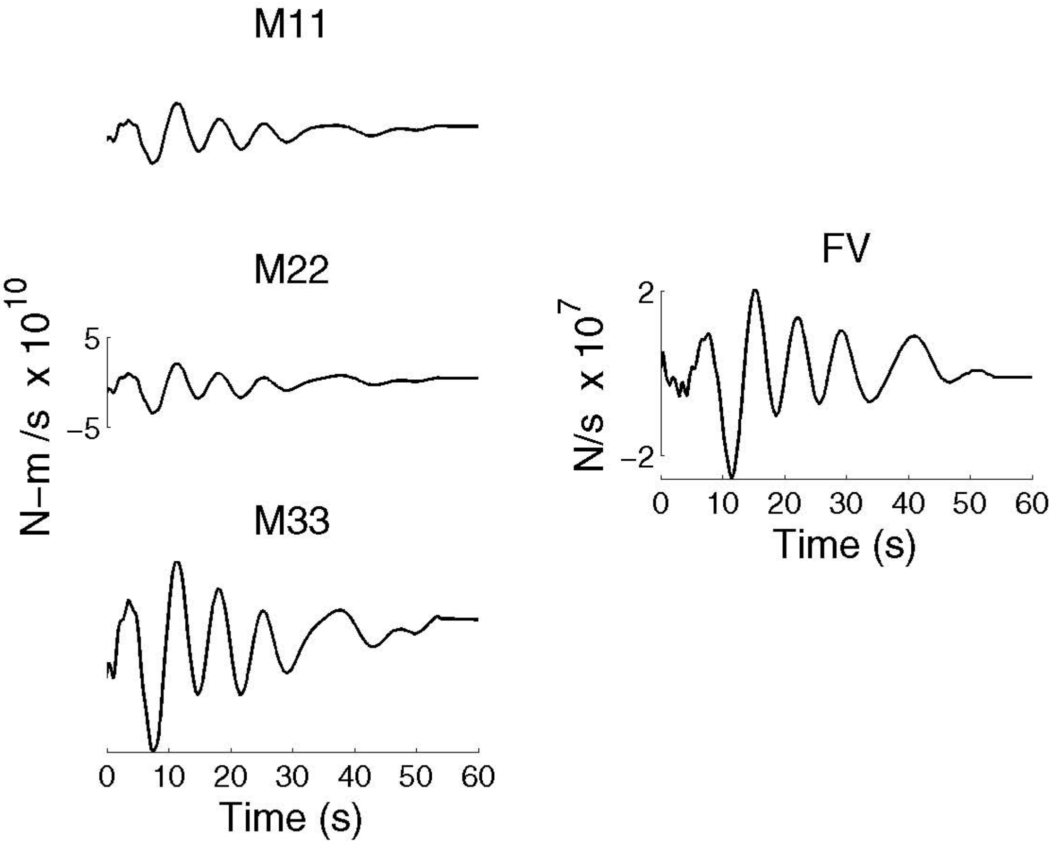

Figure 4.11: Moment rate functions for Figure 4.10, with three volumetric tensor elements and a vertical single force. The volumetric components have a maximum peak to trough amplitude ratio of [0.9:0.8:3].

| Model | Variance reduction (%) |
|---|---|
| mogi source | 21.3 |
| volumetric | 29.9 |
| volumetric + single | 61.3 |
| six couples | 47.2 |
| six couples + single | 67.4 |

Table 4.1: Waveform fit for the different models. Variance reduction calculated from equation 3.5.

| Model | AIC |
|---|---|
| Mogi source | 1.71 × 1e5 |
| volumetric | 1.90 × 1e5 |
| volumetric + single | 2.22 × 1e5 |
| six couples | 2.15 × 1e5 |
| six couples + single | 2.34 × 1e5 |

Table 4.2: AIC for the different models. AIC calculated from (4.1).

value of the AIC increases, the increase in the number of free parameters may be justifiable. Table (4.2) gives the AIC values for the different models. The model with six moment tensors and a vertical single force has the highest AIC value and is therefore the best model under this criterion.

The model using 6 couples and a single vertical force fits the observables well, however, it still has difficulties fitting certain stations, especially CON and HEL. This may be related to inaccuracies in the Green's functions caused by assuming a flat topography, as HEL and CON are near the edge of the summit plateau and are the most distant stations used. Maximum peak to trough amplitudes for the moment tensor elements in the inversion using all 6 moment tensors and a single vertical force is given in Table 4.3. Single force amplitudes of $10^{-3}$ N are roughly comparable in influence on the source to force couple amplitudes of 1 Nm [Chouet et al., 2003].

The best fit source location should give a small error to the data and have a moment rate function which is stable and fairly consistent for each component [Chouet et al., 2003]. The best location determined by these criteria is shown in Figure 4.12. This source has a depth of 100 meters.

The results for the positive (Group 1) and negative (Group 2) polarity

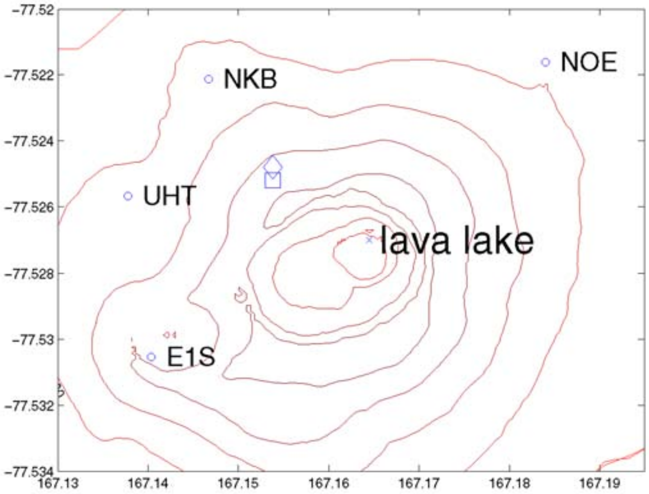

Figure 4.12: Best fit source location for the model with all six tensors and a single vertical force. Stacked and Group 1 event source shown by diamond. Group 2 event source location shown by square. Seismic stations and lava lake shown. See also Figure 1.

| $m_{11}$ | $m_{22}$ | $m_{33}$ | $m_{12}$ | $m_{13}$ | $m_{23}$ | $fv$ |
|---|---|---|---|---|---|---|
| 1.8 | 1.7 | 5.0 | 0.1 | 0.1 | 0.4 | 0.5 |

Table 4.3: Maximum peak to trough moment components in units of $10^{11}$ Nm and single vertical force in units of $10^8$ N.

events should be similar to the stacked data except at the earliest times. Due to the limited number of traces available for the Group 2 event inversion, a full inversion using 6 moment tensors and a single vertical force cannot be carried out. However, the results for the stacked data show that an inversion including only a single vertical force and the three volumetric forces is still an adequate representation of the source mechanism. The deviatoric elements are small compared to the volumetric elements and only give a slight increase in fit suggesting that the deviatoric components may not be a necessary aspect of the model.

The inversion for the Group 1 event gave the same best location as that of the stacked data. The Group 2 event gave a location which is slightly different (two grid points or 40 m south). However, due to the increased noise and decrease in number of traces, this difference may not be significant given the reduced number of constraints. Similar moment tensor ratios to the stacked inversion were found, with a maximum peak to trough ratio of [0.9:0.8:3] for the Group 1 event (Figure 4.14) and [0.7:0.9:3] for the Group 2 event (Figure 4.16). The inversion results for the coda are consistent for the different eruption types, showing that the lava lake recharging process is independent of the eruption type. The Group 2 event has a larger magnitude, as is often the case [Mah, 2003], and therefore its moment rate amplitudes are larger than the Group 1 event (see Tables 4.4 and 4.5). However, the relative amplitudes of the volumetric tensor elements are similar. The single force, however, is significantly larger (by approximately 100%) for the Group 1 event than for the Group 2.

| $m_{11}$ | $m_{22}$ | $m_{33}$ | $fv$ |
|---|---|---|---|
| 0.4 | 0.3 | 1.1 | 0.2 |

Table 4.4: Maximum peak to trough moment components for the Group 1 event. Units are in $10^{12}$ Nm and single vertical force units are $10^{9}$ N.

| $m_{11}$ | $m_{22}$ | $m_{33}$ | $fv$ |
|---|---|---|---|
| 0.3 | 0.4 | 1.3 | 0.1 |

Table 4.5: Maximum peak to trough moment components for the Group 2 event. Units are in $10^{13}$ Nm and single vertical force units are $10^{10}$ N.

It was noted that the inclination of Erebus vertical-radial VLP particle motions steepen with time during an eruption event [Rowe et al., 2000]. This effect is most apparent when the signals have been bandpass filtered in the 12 second band. To see this evolution in the moment rate function, we also bandpass filtered in the 12 second band. Looking at the maximum peak to trough amplitudes as a function of time for the stacked data, we see that the ratios of the volumetric tensors slowly change from [1.1:1.1:3] to [1:1:3]. This effect is more pronounced for the individual events. The Group 1 event has ratios evolving from [1.1:0.8:3] to [0.9:0.7:3]. For the Group 2 event, the ratio evolves from [0.7:1:3] to [0.6:0.6:3]. This shows that the source evolves with time from behaving like an isotropic source to behaving like more of a crack-like source.

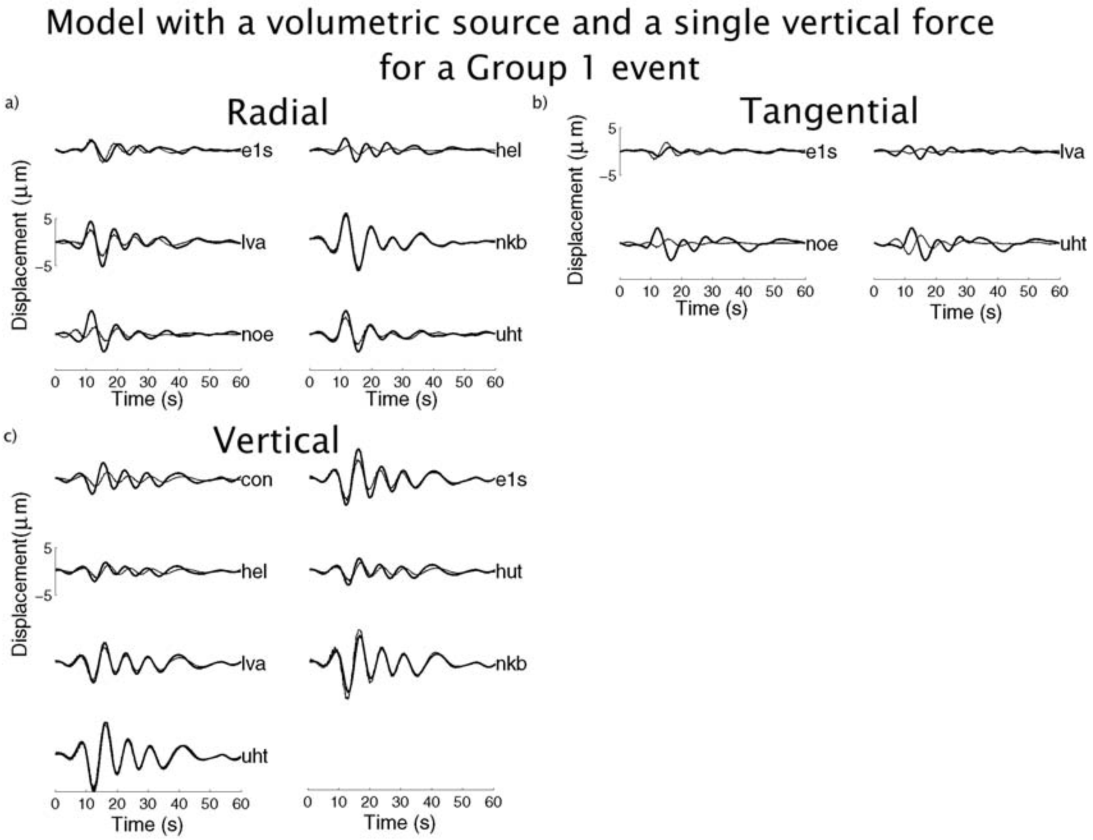

Model with a volumetric source and a single vertical force for a Group 1 event

a) Radial

b) Tangential

c) Vertical

Figure 4.13: Radial, tangential, and vertical component fit to the positive first motion event for a volumetric plus single vertical force source. Fit calculated by variance reduction. The thick lines are the observed seismograms and the thin lines are the synthetic seismograms. a) the synthetics fit 71% of the observed radial component. b) the synthetics do not fit the observed tangential component. c) the synthetics fit 84% of the observed vertical component.

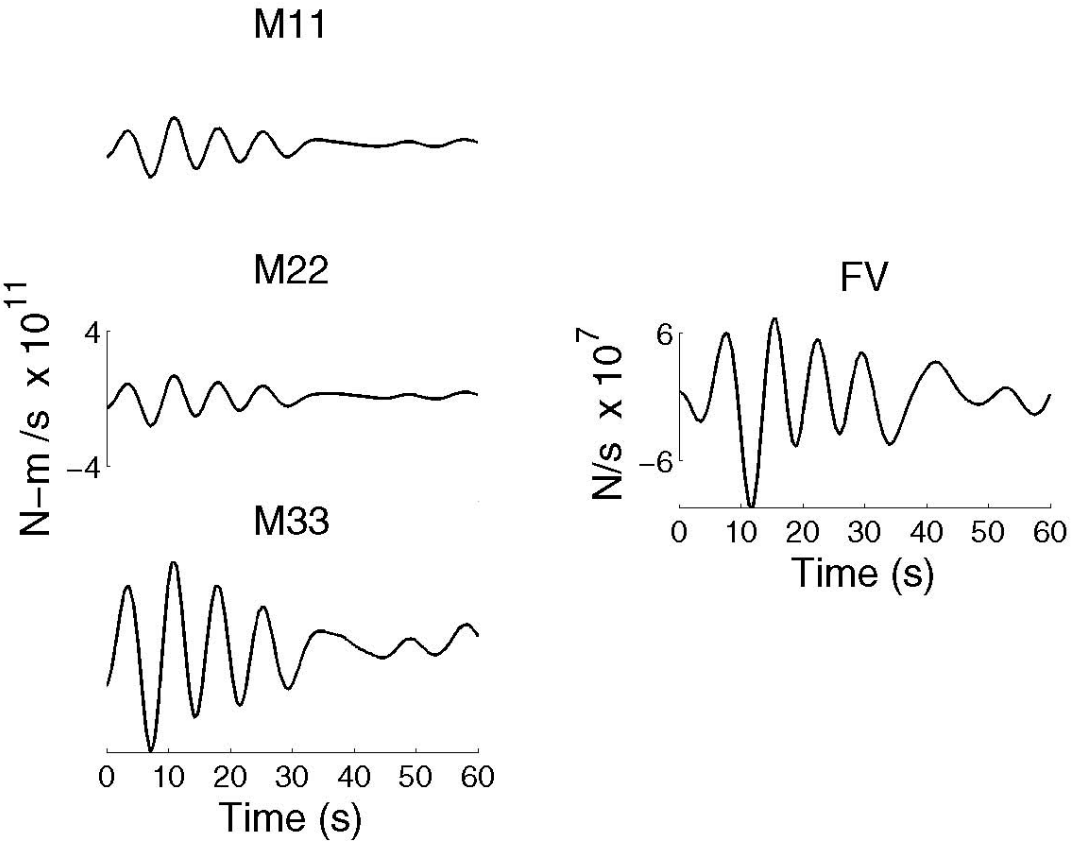

Figure 4.14: Moment rate functions for the Group 1 event (Figure 4.13).

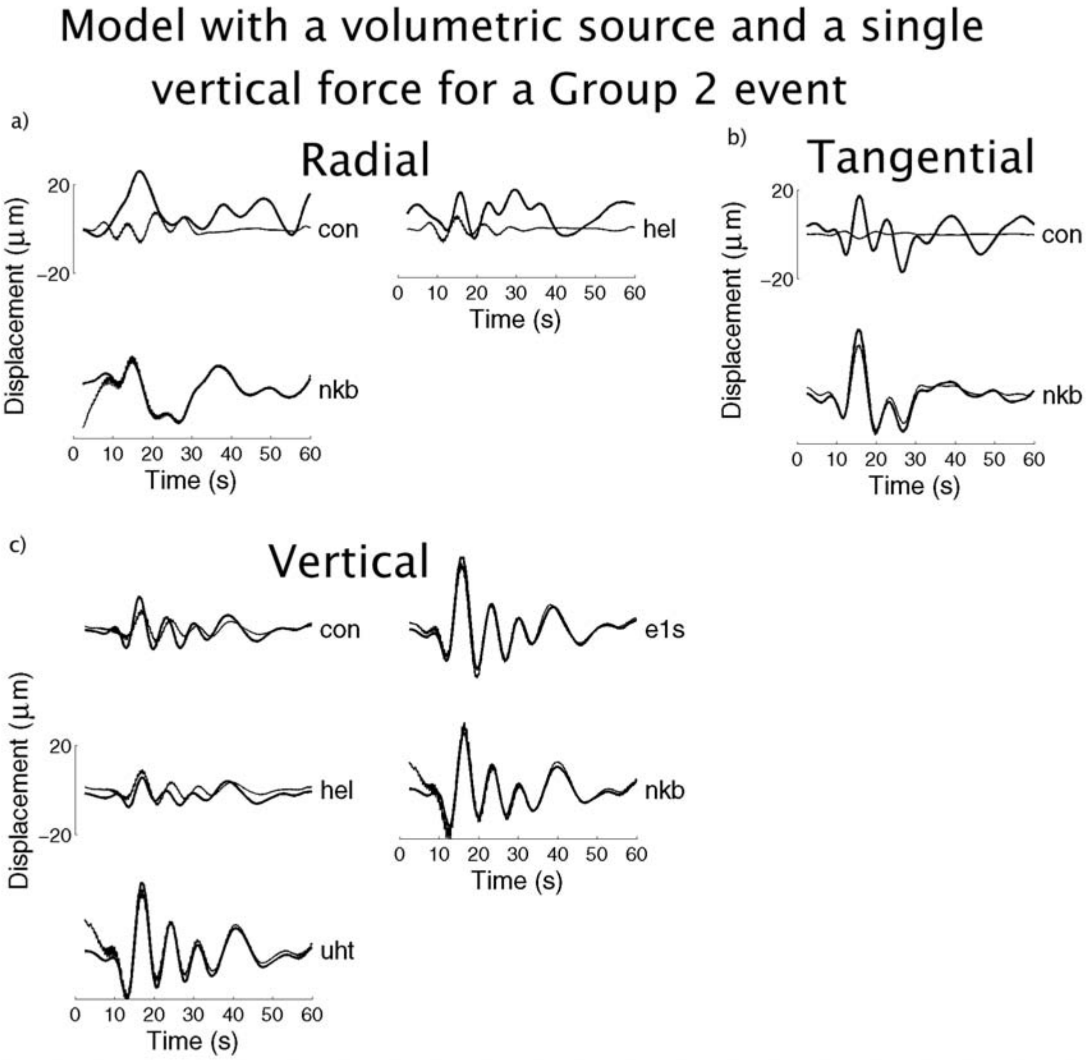

Figure 4.15: Radial, tangential, and vertical component fit to the negative first motion event for a volumetric plus single vertical force source. Fit calculated by variance reduction. The thick lines are the observed seismograms and the thin lines are the synthetic seismograms. a) the synthetics fit 10% of the observed radial component. b) the synthetics fit 50% of the observed tangential component. c) the synthetics fit 81% of the observed vertical component. Note that the signal-to-noise levels for this event, as well as the number of available traces are considerably less than for the other inversions discussed here.

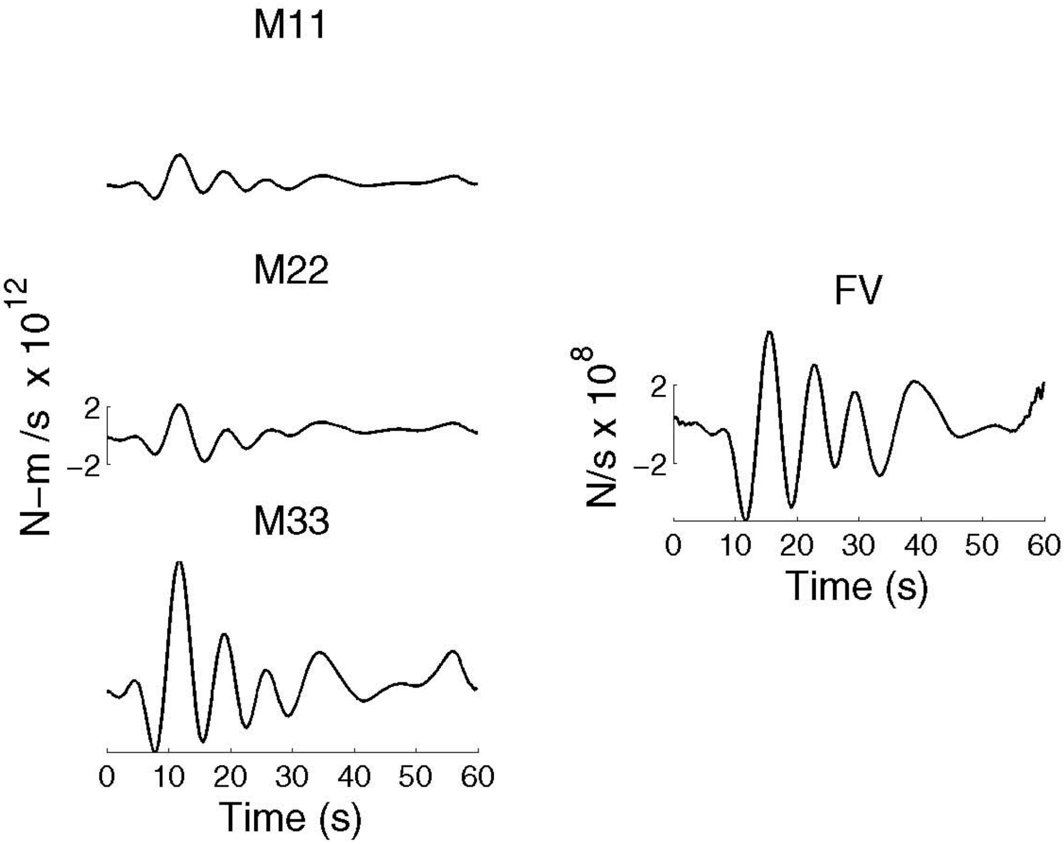

Figure 4.16: Moment rate functions for the Group 2 event (Figure 4.15).

# CHAPTER 5

## Discussion

The characteristics of seismic signals and associated moment tensors give insight into the physical source processes. The signals recorded at Erebus are shown to have sources that are dominantly volumetric and single force, and have very low frequencies relative to signals that are directly associated with explosions [Rowe et al., 2000]. Low frequency events from small volcanic source regions are often indicative of fluid movement. Tensile cracks or other conduit-associated features opening to allow fluid or gas transport have been proposed to explain source mechanisms which are dominately volumetric, ([Aster et al., 2003], [Chouet et al., 2003], [Legrand et al., 2000], [Ohminato et al., 1998], [Hidayat et al., 2002], [Kumagai et al., 2003], [Kumagai et al., 2001], [Nishimura et al., 2000]), such as seen at Erebus.

The moment tensor for a tensile crack described by the angles $\theta$ and $\phi$ (Figure 5.1) is described by Chouet [1996] as

$$M = \Delta V \begin{pmatrix} \lambda + 2\mu \sin^2\theta \cos^2\phi & 2\mu \sin\phi \cos\phi & 2\mu \sin\theta \cos\theta \sin\phi \\ 2\mu \sin^2\theta \sin\phi \cos\phi & \lambda + 2\mu \sin^2\theta \sin^2\phi & 2\mu \sin\theta \cos\theta \sin\phi \\ 2\mu \sin\theta \cos\theta \cos\phi & 2\mu \sin\theta \cos\theta \sin\phi & \lambda + 2\mu \cos^2\theta \end{pmatrix}.$$

where $\Delta V$ is the volume change. If a horizontal crack is assumed, $\theta$ is equal to zero and the tensor becomes

$$M = \Delta V \begin{pmatrix} \lambda & 0 & 0 \\ 0 & \lambda & 0 \\ 0 & 0 & \lambda + 2\mu \end{pmatrix}.$$

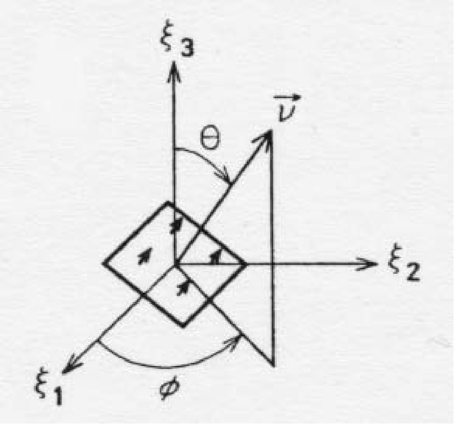

Figure 5.1: Tension crack (after Chouet, 1996).

If a Poisson solid is assumed, $\lambda = \mu$ and the ratio for a crack is described by [1:1:3]. However, if a Poisson's ratio of $\sigma = 1/3$, as is possibly more appropriate for magmatic conduit regions with low shear velocities [Chouet et al., 2003], is assumed, $\lambda = 2\mu$ and the ratio becomes [1:1:2].

Crack-like moment tensor ratios of around [1:1:3] and [1:1:2] have been found for several volcanoes. Different processes have been found to be responsible for the generation of VLP signals, but magma moving through a crack opening is involved in many explanations.

Phreatic eruptions and long period tremor events at Aso volcano in Japan were inverted for location and focal mechanism by Legrand et al. [2000]. They found that these events were mostly volumetric, with small deviatoric components. The source was part isotropic and part a vertically opening crack with a volumetric tensor ratio of [3:6:1]. They also determined that a single vertical force would not be significant because these events were not correlated with large eruptions or large amounts of internal mass transport, and only gas, water, and small rocks were ever emitted from the volcano.

VLP signals associated with dome growth were observed at Merapi volcano, Indonesia [Hidayat et al., 2002]. They found a volumetric source with a ratio of around [0.3:1:3]. They obtained a better fit to their data if they included single forces in their inversion; however, their explanation of their mechanism did not include an explanation of their single force. They suggest that the source mechanism is the degassing of rising magma as it passes through cracks in the dome interior.

VLP impulsive signals were found to be associated with magma injection at Kilauea, Hawaii [Ohminato et al., 1998]. It was found that a moment tensor ratio of around [1:1:3] or [1:1:2] fit their data, depending on which stations they used. These signals were sawtooth shaped and they were explained as gated mass transport, characterized by the slow injection of a fluid into a crack and then the rapid ejection of this fluid out of the crack, corresponding to the sharp drop in the signal. They also found a significant single vertical force. They explained this force as a drag force on the channel walls created by the flow of the magma through the crack.

Mount Hachijo Fuji, in Tokyo, revealed VLP signals following a volcano-tectonic (VT) earthquake swarm [Kumagai et al., 2003]. Moment tensor inversion revealed a vertical crack at a depth of 5 km as the source. No significant single forces were found. Kumagai et al. [2003] interpret their results as originating from a basalt-gas mixture resonating in a crack. The VT earthquake swarm and deformation of the island point towards magma injection which could feed the mixture into a dike.

Kumagai et al. [2001] found VLP signals associated with caldera formation at Miyake Island, Japan. The moment tensor ratio recovered for these signals was [0.7:1.2:6]. They explained the signal being generated by a piston-style mechanism which pushes magma from the chamber out through an outflow conduit.

A deployment of broadband seismometers in mid-1998 recorded VLP signals at Iwate Volcano, Japan [Nishimura et al., 2000]. Semblance methods and moment tensor inversion pointed to a two-point source model. No significant single force was found but a volumetric source with the $M_{xx}$ component dominating was determined. A model was proposed containing two magma chambers which are connected by a narrow conduit and sealed from each other by a valve. As the pressure in one conduit grows larger than the pressure in the second, the valve is opened to allow magma movement from the first chamber to the second. This explains their observed two-point source model with mutual deflation and inflation at the two point sources separated by 4 km.

Chouet et al. [2003] performed an inversion on the VLP signals recorded at Stromboli, Italy. They created a program for calculating Green's functions which takes into account topography and bathymetry. Again, deviatoric components were found to be minor relative to the volumetric components. Chouet et al. [2003] performed the inversion with all 6 moment tensors and all three single forces to find a ratio of [1:1:2] for their volumetric components. They also found a significant vertical single force.

Based on the results from other volcanoes, the VLP signals from Erebus likely represent magma passing through a subhorizontal crack-like geometry. The mechanism is possibly similar to the one described for magma injection under Kilauea by Ohminato et al. [1998]. For the scenario at Erebus, gas bubbles will continue to coalesce and grow inside of a crack, inflating the crack and displacing magma. Once a critical buoyancy threshold is reached the bubble is released. It then rises to the surface, where it decompresses explosively at the lava lake surface. The slight change over roughly 40 s in moment tensor ratios from [1.1:0.8:3] to [0.9:0.7:3] for Group 1 events during the ensuing VLP signal and from [0.7:1:3] to [0.6:0.6:3] for Group 2 events is indicative of an evolving source. During this period the source slowly evolves from having a more isotropic component to more of a crack source. The shear components were found to be minor compared to the volumetric components. This is not surprising as the source involves gas and fluid movement and a mechanism for exciting shear waves is not readily apparent.

The importance of a single force in fitting the data at Erebus appears valid, using an explanation similar to the one that Chouet et al. [2003] used for the existence of single forces at Stromboli. The presence and physical interpretation of single forces without external mass ejection was explained by Takei and Kumazawa [1994], where a single force can be created due to a momentum exchange. Inside a given region, if dense material moves down and less dense material moves up, gravitational energy will be released. A reaction force to this gravitational pulse creates a single force. This will result in a positive single vertical force during this acceleration phase. During the deceleration phase, there will be a negative vertical single force. To have conservation of momentum, the upward and downward single forces must cancel out so that the time integral of the single force over the event vanishes.

For example, Chouet et al. [2003] observed a single vertical force associated with strombolian eruption events at Stromboli. This single force first has a negative pulse and then a positive one. They explain that the gas bubble which is released from a feeder dike first perches the magma above it up to make space for the bubble. Then the bubble moves up the conduit and the magma pushes down past the bubble to fill the void created by the bubble. This acceleration of magma first up and then down creates the reactionary single force of first a negative and then a positive motion.

Chouet et al. [2003] also observed that their negative single force correlates with volume inflation and their positive single force correlates with volume deflation, as is consistent with the out of phase relationship seen at Erebus (Figure 5.2). The coda of the Erebus VLP signal represents the lava lake recharging stage. During this stage, magma rushes into the conduit to fill the void recently made by the eruption. This creates a reactionary negative vertical force.

The mechanism could be similar to that found at Kilauea [Ohminato et al., 1998]. A drag force was used to describe the single force, due to the magma passing through narrow conduit walls. The shape of the waveform of the single force found at Kilauea is quite different for that found at Erebus, however. At Erebus, the single force is oscillatory with an equal negative and positive contribution. For Kilauea, the single force is a positive pulse shape. Ukawa and Ohtake [1994] found a traction force responsible for an earthquake which preceded a volcanic eruption of Izu-Ooshima. They model

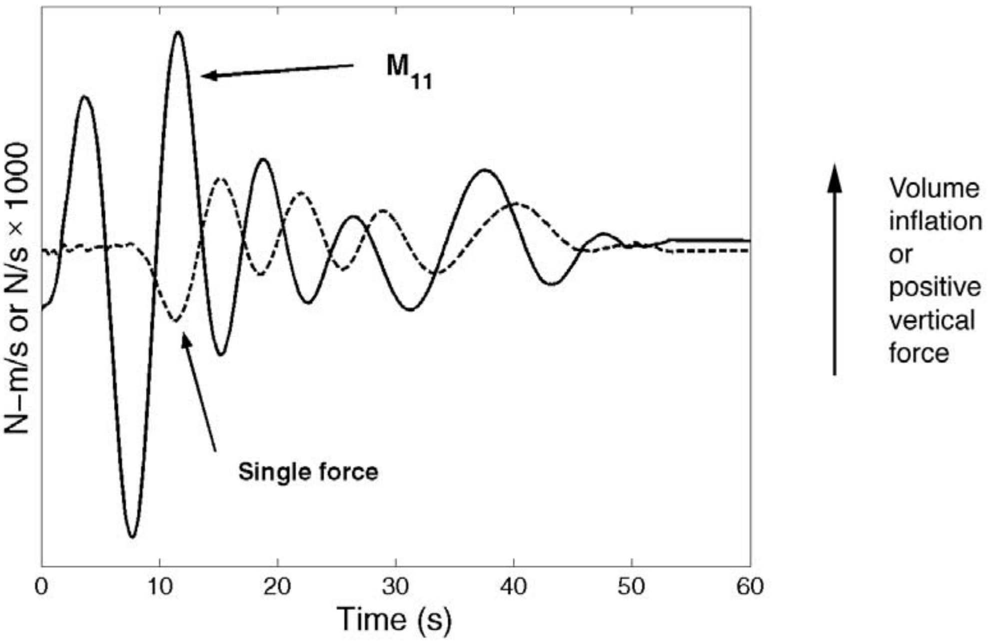

Figure 5.2: The $M_{11}$ and single force moment and force rate functions for the stack event. The single force has been multiplied by 1000 to give it a comparable numerical amplitude.

magma transport from one conduit to another due to a lower pressure in the second conduit. For Erebus, the sudden evacuation of magma from the lava lake would create a lower pressure condition. As the magma moves from a lower reservoir to recharge the lava lake, this drag force would be applied. The magma might be modulated by a subhorizontal crack which separates the two reservoirs and opens only when pressures are great enough. The magma would move up in a sluggish form, pushing into the lava lake, then relaxing a little, to then push upwards again. This surging recharge of the magma would create the observed oscillatory VLP signal observed.

The processes which happen in the initial several seconds of the VLP

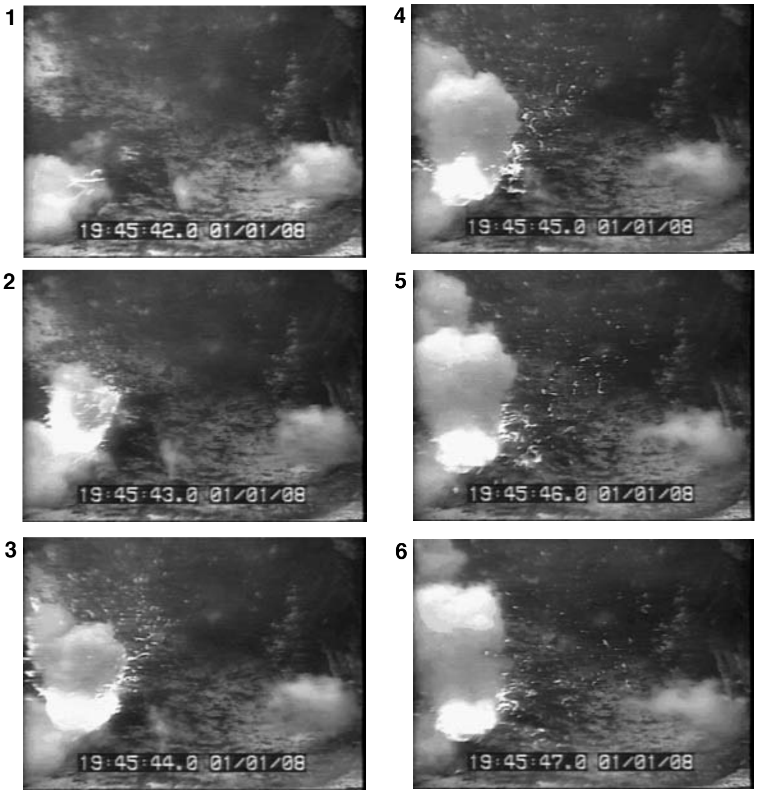

Figure 5.3: Lava lake video camera footage showing a Group 1 (positive vertical first motion) eruption. The eruption style has a distinctly jet-like vertical component. Compare with Figure 5.4 (After Mah, 2003).

event are not as clear, however. The differences between the mechanisms of Group 1 and Group 2 events are very interesting and corroborate work by Mah [2003], who found that there was a systematic difference in the eruption styles of the two events from viewing video footage [Mah, 2003] (Figures 5.3 and 5.4) of the eruptions. He found that the positive polarity events (Group 1) have a distinctly jet-like vertical component to their ejecta while the negative polarity events (Group 2) are more radial and asymmetric (to the west).

This eruption difference can be seen in the different single forces of

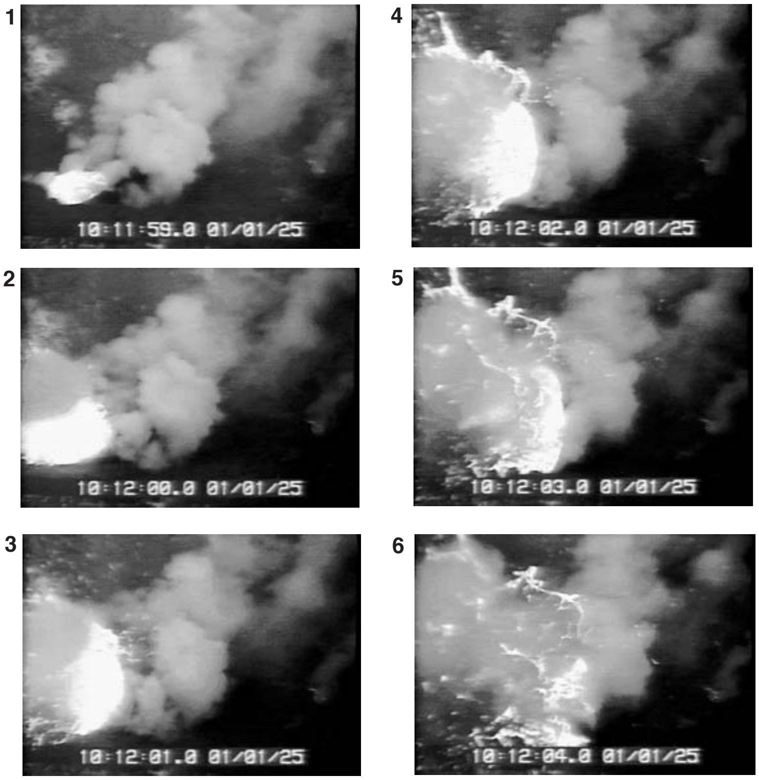

Figure 5.4: Lava lake video camera footage showing a Group 2 (negative vertical first motion) eruption. The eruption style has a radial and asymmetric component. Compare with Figure 5.3 (After Mah, 2003).

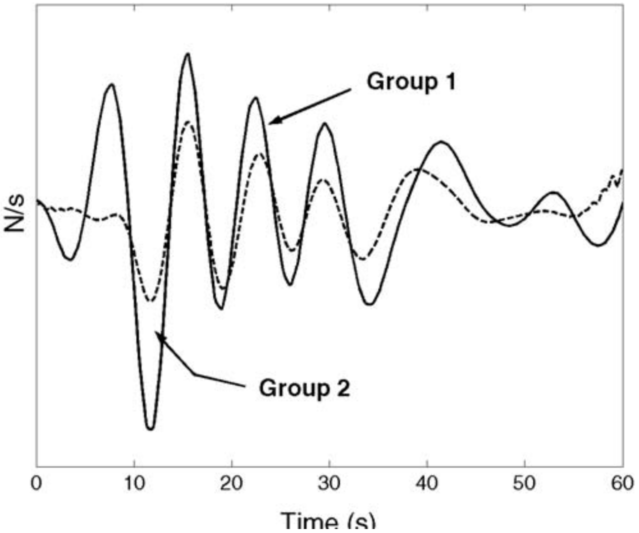

Figure 5.5: The single force rate function for the Group 1 (solid line) and Group 2 (dashed line) event.

the two events. The Group 1 event has an approximately 100% larger (when normalized by the mean amplitudes of the volumetric tensor components) amplitude single force than the Group 2 event (Figure 5.5). Another interesting feature is that the single force for the Group 2 event is greatly reduced for the first several seconds of the seismic signal (Figure 5.6(b)). However, for the Group 1 event, the single force initiates strongly at the same time as the volumetric components (Figure 5.6(a)). The late start of the single force for the Group 2 event suggests that the single force is only an important factor during the aforementioned resurgent lava lake recharging process. However, a single force appears to be a necessary factor in the pre-eruptive and eruptive stages in the Group 1 event.

According to Chouet et al. [2003], the observed single force at Strom-

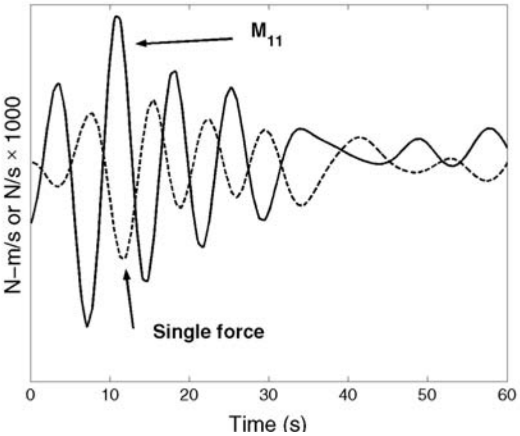

(a)

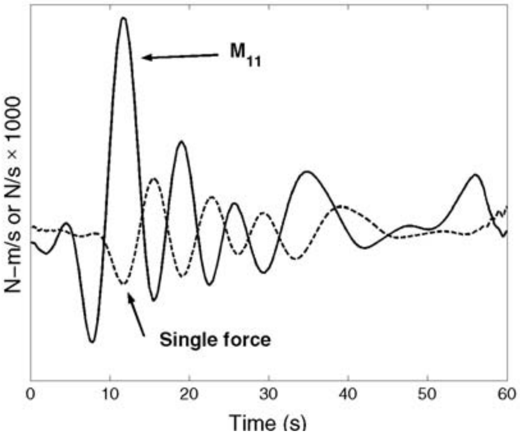

(b)

Figure 5.6: The $M_{11}$ moment and single force rate functions for the (a) Group 1 and (b) Group 2 event. The single force has been multiplied by 1000 to give it a comparable numerical amplitude.

boli was due to the interaction of a large gas bubble and the magma through a crack-like conduit system. It would seem from this explanation that a single force would always be apparent in a strombolian style eruption. However, in the explosive stage of some eruptions at Erebus only the Group 1 events show this feature.

To gain a better understanding of eruption processes, the factors which control creation and magnitude of the single force must be determined. Factors involved could include, but are not limited to, the source location, the ascension velocity, the bubble size, the bubble shape, and the magma and bubble content.

The inversion of the Group 1 and 2 events showed almost the same source location as the stacked data (with the Group 2 event differing by only 40 m south). Given the small number of traces used for the Group 2 event, this source location difference could be an artifact of insufficient data and higher noise levels and may not be significant. This, along with the stability of incident angles studied by Mah [2003], suggests that the centroid moment tensor source location is stationary and that if two separate source locations do exist, they are close to each other.

The depths of the source locations may be different, since depth is not easily constrained. The two bubble coalescence areas are probably within the same conduit and are created by small irregularities within the conduit. A slight incline to the conduit [James et al., 2004] or a small roughness to the conduit [Jaupart and Vergniolle, 1988] is all that is necessary to instigate bubble coalescence. If the bubble responsible for the Group 2 event coalesces at a shallower depth, and at a more oblique angle, this could explain the differences in eruption styles observed. The shallower source would create less of a gravitational disturbance and would therefore not create as large of a vertical single force. The oblique trajectory of the bubble would create the asymmetrical radial ejecta, rather than the vertical ejecta produced by bubbles for the Group 1 events (Figure 5.7).

Further observations, both in the laboratory and of actual events, are necessary to address some of the ambiguity about factors controlling the generation of a single force moment rate function. Some of the previous studies on VLP events mentioned earlier, such as Legrand et al. (2000), dismissed the consideration of a single force in their inversion because no significant ejecta resulted from the event. However, it has been shown that single force components can be created deeper within the conduit without any extrusion or external forces necessary ([Takei and Kumazawa, 1994] and [Chouet et al., 2003]), although in this case they must integrate to zero with time. This is not to suggest that a single force will be present. Our data shows that during the eruptive stages of the signal, explosions with varying sizes of single force rate function exist.

Several factors can limit our results, including source mislocation, data coverage, and inaccurate Green's functions. In general, it was found in our synthetic tests that a source mislocation of one node in the horizontal or vertical direction affected the amplitudes of different components of the moment rate function and in different ways. However, the relative amplitudes remained basically the same so that the source mechanisms were still recovered, and

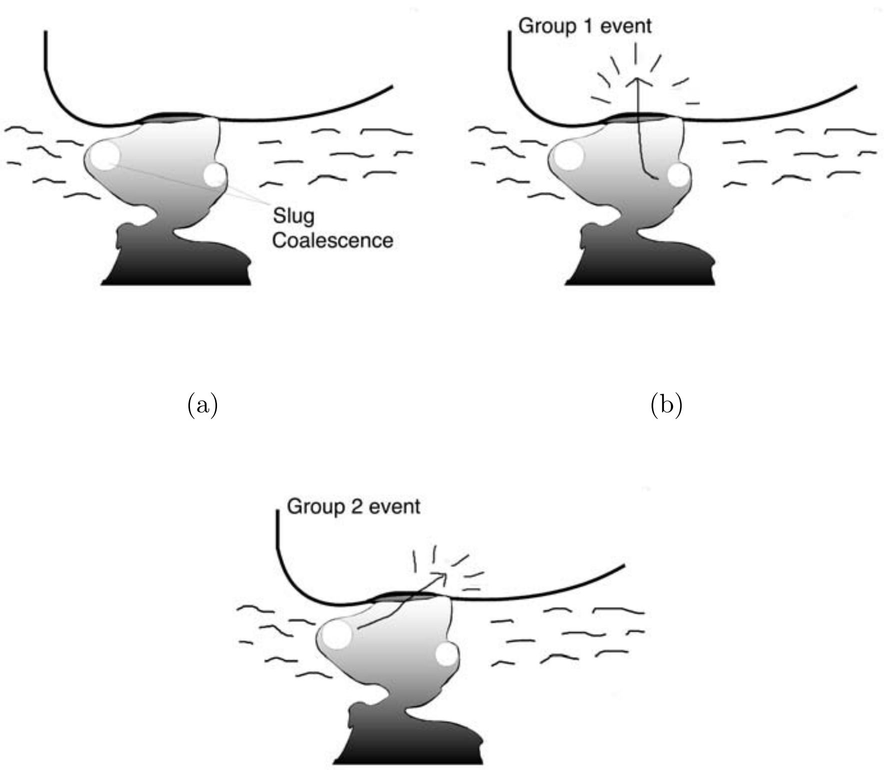

(a)

(b)

(c)

Figure 5.7: a) Possible conduit geometry. Two separate locations of bubble coalescence determine if an event is Group 1 or Group 2. b) Bubble coalescence and subsequent rise and decompression creating jet-like vertical ejecta characteristic of a Group 1 eruption. c) Bubble coalescence and subsequent rise and decompression from an oblique angle, creating radial ejecta characteristic of a Group 2 eruption.

the amplitude of the single force was not greatly affected. Therefore, we have confidence that a source mislocation of this magnitude would not greatly change our results. Tests also showed that a spurious single force could be modeled due to a source mislocation. However, due to the poor fit of the synthetics without a single force and the decrease of the AIC number, we conclude that the single force component is a necessary feature of the model and not just an artifact of a source mislocation.

Inaccuracies in the Green's functions poses a potentially more significant problem. For the analytical calculation of Green's functions, a homogeneous half-space with flat topography is assumed. This is a large simplification of the topographic and internal structure of Erebus and so our confidence in our Green's functions is limited. Often topography can be ignored when calculating Green's functions for the purposes of inverting for earthquake source mechanisms. However, the dramatic topography of volcanoes tends to make this a more important consideration [Chouet et al., 2003]. Ohminato and Chouet (1997) performed a study where they used a method to include topography into the calculation of wave propagation. They found that there were significant differences in the calculations for some simple topographic structures. For concave features, they found that phases were generated in the 3-D calculation from the incident S-wave interacting with the corners of the feature. These phases were absent in the 2-D calculation. The interference of these waves with other phases affected much of the later propagation of the waves. For convex features, such as might represent a volcano, they found that the wave energy is focused along areas with greatest topographic relief.

The effects of topography will probably be most important for stations which are situated near a steep slope. The edge effects of the seismic wave hitting this gradient could have a noticeable effect on the Green's functions. Therefore, the calculations of Green's functions which take topography into account, such as was done at Stromboli, could increase the accuracy of the results. Future work should include further investigation of this issue. Inversion results for stations CON and HEL both show a systematic underestimation of the amplitude of traces compared to the observed traces. These stations are situated close to steep slopes; if the topography creates a focusing of seismic energy here, we would not observe it with our simple half-space flat topography Green's functions.

Another problem to consider is the azimuthal coverage. Ideally, 360 degree azimuthal coverage is preferred to best recover and constrain the true focal mechanism. For example, Hidayat et al. (2002) suggested that the low value of one of their principle axes was an artifact of poor station coverage. However, at Erebus, better azimuthal coverage is simply not an option due to the difficult conditions that occur on the southern parts of the mountain at higher elevations. Future deployments should be considered there as conditions allow.

Future work may also help to determine the depths of the coalescence areas for the Group 1 and Group 2 events. Using infrasound observations, the differences in the amount of overpressure existing in the bubbles for the two types of eruption events could lead to insight into the depth of the bubble coalescence and the velocity at which the bubble rises to the surface. Another possible area of future work is to investigate the relationship of the three spectral peaks consistently observed in the VLP signals to the eruption mechanics. The implications of the spectral peaks are not yet understood.

# CHAPTER 6

# Conclusion

The moment rate and force rate functions determined at Erebus are consistent in some ways with results found at other volcanoes with VLP signals. The dominantly volumetric source with a maximum peak to trough ratio of [1.1:1:3] is consistent with the excitation of a subhorizontal crack. The initial gas bubble and subsequent mass transport exerts pressure against the walls of the conduit. This slug is then released and rises quickly to the surface of the lava lake where it decompresses explosively, spraying the inner crater with ejecta. The volumetric expansion and contraction continues as the lava lake regains equilibrium through an extended oscillatory mechanism. The volumetric ratio evolves slightly with time, suggesting that the process changes from having an isotropic source component to a purely crack source. It does remain roughly [1:1:3], throughout the first 60 seconds of signal, suggesting that the new magma which has entered into the chamber to fill the void created by the eruption also enters through a crack.

During the lava lake recharging process, a pressure difference caused by the removal of lava lake material in the eruption will force magma to move up from a deeper reservoir into the lake reservoir. The magma is transported unsteadily, but in an oscillatory and repeatable way. The initial acceleration of magma upwards and into the lake reservoir creates a negative single vertical force rate function. The oscillatory deceleration causes the single force rate function to swing to the opposite direction. When the next pulse of magma comes from below, the process starts again, so that the result is an oscillatory single force with decreasing amplitude as the lake approaches a resumed equilibrium.

The initial few seconds of the event has much more variability than the extended refill-associated coda. For events with positive initial polarity, there is a strong vertical single force which begins immediately with VLP signal onset. This single force is approximately two times larger than the single force associated with negative initial polarity events, after normalizing for event magnitude. In addition, the single force for negative polarity events is negligible for the initial stages of the event associated with the gas bubble transport.

The Group 1 event has a more vertical jet-like eruption, as seen in video footage while the negative event has a more radial eruption [Mah, 2003]. We conclude that differences in the gas slug or slug ascension create differences in the type of eruption and mechanisms observed, so that a single vertical force plays a role in the eruptive mechanism of positive polarity events but not for negative polarity events. One possibility is that the conduit contained two nucleation sites for gas slugs during 1999-2001. One of these sites delivered gas slugs in a more lateral manner, perhaps from a more shallow depth, resulting in less initial gravitational potential release. This source region would correspond to Group 2 events. The second site delivered more vertically-traveling slugs with greater gravitational potential release during ascension. This source region corresponded to Group 1 events. The extended oscillatory VLP coda corresponds to a recharge process that is insensitive to the eruption, hence explaining its repeatability.

# REFERENCES

[Akaike, 1974] Akaike, H. (1974). A New Look at the Statistical Model Identification. *IEEE Transactions on Automatic Control*, AC-19(6):716–723.

[Aki and Richards, 2002] Aki, K. and Richards, P. (2002). *Quantitative Seismology.* University Science Books, 2nd ed edition.

[Arciniega-Ceballos et al., 1999] Arciniega-Ceballos, A., Chouet, B., and Dawson, P. (1999). Very-Long-Period signals associated with vulcanian explosions at Popocatepetl Volcano, Mexico. *Geophysical Research Letters*, 26(19):3013–3016.

[Aster et al., 2003] Aster, R., Mah, S., Kyle, P., McIntosh, W., Dunbar, N., Johnson, J., Ruiz, M., and McNamara, S. (2003). Very Long Period Oscillations of Mount Erebus Volcano. *Journal of Geophysical Research*, 108(B11, 2522).

[Aster et al., 2004] Aster, R., McIntosh, W., Kyle, P., Esser, R., Bartel, B., Dunbar, N., Johns, B., Johnson, J., Karstens, R., Kurnik, C., McGowan, M., McNamara, S., Meertens, C., Pauly, B., Richmond, M., and Ruiz, M. (2004). New instrumentation delivers multidisciplinary real-time data from mount erebus, antarctica. *EOS trans. AGU*, 85(10).

[Chouet, 1996] Chouet, B. (1996). *Monitoring and Mitigation of Volcano Hazards*, chapter New Methods and Future Trends in Seismological Volcano Monitoring. Springer-Verlag.

[Chouet et al., 2003] Chouet, B., Dawson, P., Ohminato, T., Martini, M. andSaccorotti, G., Giudicepietro, F., De Luca, G., Milana, G., and Scarpa, R. (2003). Source mechanisms of explosions at Stromboli Volcano, Italy, determined from moment- tensor inversions of very-long-period data. *J. Geophys Res.*, 108(B1 2019).

[Dibble et al., 1994] Dibble, R., O'Brien, B., and Rowe, C. (1994). The Velocity Structure of Mount Erebus, Antarctica, And It's Lava Lake. In Kyle, P., editor, *Volcanological and Environmental Studies of Mount Erebus, Antarctica*, volume 66 of *Antarctic Research Series*, pages 1–16. AGU.

[Hagerty et al., 2000] Hagerty, M., Schwartz, S., Garces, M., and Protti, M. (2000). Analysis of seismic and acoustic observations at Arenal Volcano, Costa Rica, 1995 1997. *Journal of Volcanology and Geothermal Research*, 101:27–65.

[Hidayat et al., 2002] Hidayat, D., Chouet, B., Voight, B., Dawson, P., and Ratdomopurbo, A. (2002). Source mechansim of very-long-period signals accompanying dome growth activity at Merapi volcano, Indonesia. *Geophysical Research Letters*, 29(23).

[James et al., 2004] James, M., Lane, S., Chouet, B., and Gilbert, J. (2004). Pressure changes associated with the ascent and bursting of gas slugs in liquid-filled vertical and inclined conduits. *Journal of Volcanological and Geothermal Research*, 129:61–82.

[Jaupart and Vergniolle, 1988] Jaupart, C. and Vergniolle, S. (1988). Laboratory models of hawaiian and strombolian eruptions. *Nature*, 331:58–60.

[Johnson et al., 2003] Johnson, J., Aster, R., Ruiz, M., Malone, S., McChesney, P., Lees, J., and Kyle, P. (2003). Interpretation and utility of infrasonic records from erupting volcanoes. *Journal of Volcanology and Geothermal Research*, 121:15–63.

[Johnson, 1974] Johnson, L. R. (1974). Green's Function for Lamb's Problem. *Geophys. J. R. astr. Soc.*, 37:99–131.

[Kanamori et al., 1984] Kanamori, H., Given, J., and Lay, T. (1984). Analysis of seismic body waves excited by the mount st. helens eruption of may 18, 1980 ( usa). *Journal of Geophysical Research*, 89(B3):1856–1866.

[Kumagai et al., 2003] Kumagai, H., Miyakawa, K., Negishi, H., Inoue, H., Obara, K., and Setsugu, D. (2003). Magmatic Dike Resonances Inferred from Very-Long-Period Seismic Signals. *Science*, 299:2058–2061.

[Kumagai et al., 2001] Kumagai, H., Ohminato, T., Nakano, M., Ooi, M., Kubo, A., Inoue, H., and Oikawa, J. (2001). Very-Long-Period Seismic Signals and Caldera Formation at Miyake Island, Japan. *Science*, 293:687–690.

[Lay and Wallace, 1995] Lay, T. and Wallace, T. C. (1995). *Modern Global Seismology*. Academic Press.

[Mah, 2003] Mah, S. (2003). Discrimination of Strombolian eruption types using very long period (VLP) seismic signals and video observations at Mount Erebus, Antarctica. Master's thesis, New Mexico Institute of Mining and Technology.

[Mogi, 1958] Mogi, K. (1958). Relations between the eruptions of various volcanoes and the deformations of the ground surfaces around them. *Bull. Earthquake Res. Inst. Univ. Tokyo*, 36:99–134.

[Nishimura et al., 2000] Nishimura, T., Nakamichi, H., Tanaka, S., Sato, M., Kobayashi, T., Ueki, S., Hamaguchi, H., Ohtake, M., and Sato, H. (2000). Source Pcoress of Very Long Period Seismic Events Assocated with the 1998 Activity of Iwate Volcan, Northeastern Japan. *Journal of Geopphysical Research*, 105(B8):19135–19147.

[Ohminato et al., 1998] Ohminato, T., Chouet, B., Dawson, P., and Kedar, S. (1998). Waveform inversion of very long period impulsive signals associated with magmatic injection beneath Kilauea Volcano, Hawaii. *Journal of Geophysical Research*, 103(B10):23,839–23,862.

[Ohminato and Chouet, 1997] Ohminato, T. and Chouet, B. A. (1997). A Free-Surface Boundary Condition for Including 3D Topography in the Finite-Difference Method. *Bulletin of the Seismological Society of America*, 87(2):494–515.

[Rothery and Oppenheimer, 1994] Rothery, D. and Oppenheimer, C. (1994). Monitoring Mount Erebus By Satellite Remote Sensing. In Kyle, P., editor, *Volcanological and Environmental Studies of Mount Erebus, Antarctica*, volume 66 of *Antarctic Research Series*, pages 51–56. AGU.

[Rowe et al., 2000] Rowe, C. A., C., A. R., Kyle, P. R., Dibble, R. R., and Schlue, J. W. (2000). Seismic and acoustic observations at Mount Erebus Volcano, Ross Island, Antarctica, 1994-1998. *Journal of Volcanology and Geothermal Research*, 101:105–128.

[Takei and Kumazawa, 1994] Takei, Y. and Kumazawa, M. (1994). Why Have The Single Force and Torque Been Excluded from Seismic Source Models? *Geophysical Journal International*, 118:20–30.

[Tazieff, 1994] Tazieff, H. (1994). Preface. In Kyle, P., editor, *Volcanological and Environmental Studies of Mount Erebus, Antarctica*, volume 66 of *Antarctic Research Series*, pages xi–xii. AGU.

[Ukawa and Ohtake, 1994] Ukawa, M. and Ohtake, M. (1994). A Monochromatic Earthquake Suggesting Deep-seated Magmatic Activity Beneath Izu-Ooshima volcano, Japan. *Journal of Geophysical Research*, 92:17757–17773.